3D-modelling of turbulent flow and bed shear stress around vegetation: Effects of scour and bending

Master Thesis

University of Twente

H. Buijs	S2352230
Daily supervisor	Dr. ir. T.J. (Thomas) van Veelen
Daily supervisor	Dr. ir. V. (Vasileios) Kitsikoudis
Head of committee	Dr. ir. B.W. (Bas) Borsje

26th March 2025

Foreword

This thesis is the final part of my time at the University of Twente. The thesis has been carried out at the department of Civil Engineering. I hope that the effect of bending of vegetation will be more applied in the field in the near future.

I would like to thank the members of the graduation committee for their supervision and the suggestions to improve my report. First, I would like to thank Thomas van Veelen for all his feedback on both the report and presentations. Second, I would like to thank Vasileios Kitsikoudis for his critical review of the report and on with his focus on the knowledge gap. Both daily supervisors were very helpful and motivating during times that the model did not work as expected. They kept me motivated, which ultimately got the work done. The positivity they brought during the master thesis was very welcome. Last, I would like to thank Bas Borsje for his feedback that gave a different perspective on the report, where the focus was on who to write for.

Further, I would like to thank my family, friends and fellow students for their support during the study and master thesis. A special thanks to Bas and Michiel for reviewing my master thesis and their feedback.

Abstract

Salt marshes and vegetated foreshores have recently obtained more attention. The functions of these vegetated planes are to stabilize the coastline and reduce the flood risk (Temmerman et al., 2023). Sediment transport within the salt marsh happens at lower velocities, due to the vegetation. The erosion of a salt marsh can therefore threaten the flood safety provided by the salt marsh. In several studies the vegetation has been simplified to cylinders (e.g. Baptist et al., 2007; Baptist et al., 2005; Conde-Frias et al., 2023; Etminan et al., 2018). Some studies focused on a straight cylinder and the scour around a cylinder (e.g. Aksel et al., 2021; Kirkil et al., 2008; Roulund et al., 2005). Based on the studies with scour can be concluded that the effect on the flow field and bed shear stress. Since the bending of vegetation is important for the wave attenuation (Temmerman et al., 2023) and flow field. Others focused on the inclination of a cylinder (e.g. Aksel, 2023; Kitsikoudis et al., 2017; Wang et al., 2020). The inclination of a cylinder also alters the flow field. This leaves two important factors for the alteration of the flow, which are bending and scour. This leaves a knowledge gap in what the combined effect is of scour and inclination on the flow field and bed shear stress. This leads to the research question, which is: "How does the bending of vegetation and scour of the bottom affect the flow structure and bed shear stress?". The cases were with an inclination angle of 0° and 14° and a flat bed and scoured bed simulation, leading to four cases in total. The problem has been modelled using a RANS $k-\omega SST$ model in OpenFOAM. The model has been validated on the experimental data of Kitsikoudis et al. (2017). The validation was for the main regions within 10% of the normalized velocities. The flow field changes for an inclined cylinder. For a straight cylinder the upstream flow bends down upstream of the cylinder resulting in the HV. The flow crosses the cylinder horizontally. Close to the bottom the HV reconnects downstream of the cylinder. In the wake the main fluctuations are in transverse and streamwise direction. For the inclined cylinder the flow partially bends upwards resulting in a weaker HV. Instead of crossing the cylinder horizontally, the flow crosses the cylinder under an angle. Further is there an increase in vertical velocity behind the cylinder. The TKE also decreases for the inclined case, where vertical fluctuations had the largest contribution to the TKE. The introduction of scour resulted in an additional HV inside the scour hole. The scour hole reduces the bed shear stress in the scour hole. Downstream of the scour hole, sediment deposition ridge is formed. At this location the bed shear stress has therefore increased compared to the flat bed case. The bed shear stress is around the same order, but the largest bed shear stresses were measured inside the scour hole. Compared to the bed shear stress amplification is the bed shear stress fluctuation relatively small. In the flow field the TKE decreases due to scour and inclination. However, the simulation with an inclined cylinder and scoured bed showed some discrepancies. To conclude the bending of vegetation ans scour around the vegetation is important as it lowers the capacity for sediment transport, meaning that salt marshes will be more stable over time.

Contents

List of Figures

Chapter 1
Introduction

1.1 Problem context

Floodings are a problem that have always existed in human history. Climate change has put even more pressure on the flood safety in the world. This has resulted in the need for solutions that improve our flood safety and are beneficial for the climate. While in the past, often hard solutions, like dikes and dams, were used for flood protection. Nowadays nature-based solutions play an important role in flood safety. One of those nature based solutions is a salt marsh, which serves the purpose of attenuating waves and currents, as well as stabilizing the coastline (Temmerman et al., 2023). The salt marsh vegetation dissipates the wave energy and energy from the current, leading to a reduction in wave height and flow velocity. Therefore the flood safety is increased compared to a bare bed. The salt marsh vegetation also affects the sediment transport. Compared to a bare bed the critical velocity for sediment transport initiation decreases (van Veelen et al., 2025; Zanke, 2003). The decrease in the critical value for sediment transport initiation is caused by the turbulence in the water generated by the interaction between the flow and the vegetation (Zanke, 2003). Therefore, turbulence increases the capacity for sediment transport within a salt marsh for low velocities (Baptist, 2003). The sediment transport leads to either an expansion or retreat of the salt marsh. The retreat or expansion of the salt marsh is important to understand due to the function of salt marshes in flood protection. Every tide sediment is transported over the salt marsh. Depending on the water level the vegetation is emerged or submerged in the water. The tide and current also exert a force on the vegetation itself. For moderate to calm weather conditions the vegetation might slightly bend in the flow direction. How large the bending is depends on the stiffness of the vegetation and the flow velocity. The bending of vegetation results in a smaller frontal area, which reduces the flow resistance (Baptist et al., 2007) and reduces the capacity for wave attenuation (Temmerman et al., 2023). For storm conditions, the bending of the vegetation might increase even more and this could lead to the vegetation being uprooted and being transported with the flow.

Vegetation can have complex dynamics. For example, bending in the flow direction or the interaction of the leaves with the flow. These interactions are difficult to model and make it hard to understand the dynamics around vegetation. Hence vegetation is often simplified (Vargas-Luna et al., 2016). Depending on the type of vegetation, vegetation can be defined as a stem with (some) leaves. Leaves can have a significant influence on the flow, depending on the processes that are studied (Nepf & Ghisalberti, 2008; Vargas-Luna et al., 2016). If the focus is on the resistance of the stem of vegetation, the leaves can be neglected, meaning that vegetation can be simplified as a cylinder (Nepf & Ghisalberti, 2008). Baptist et al. (2005) suggest that the representation of vegetation as a cylinder leads to a more accurate bed shear stress compared to applying a bed roughness on a flat bed. Another simplification that can be made is that the vegetation is not flexible, resulting in a rigid cylinder representing the vegetation.In the previous section is mentioned that the vegetation is able to bend with the flow. Vargas-Luna et al. (2016) noted that the bending of vegetation plays an important role in the flow resistance. However, as the bending has a large effect on the

flow (Kitsikoudis et al., 2017; Wang et al., 2020, e.g.) a slightly inclined rigid cylinder might be able to give a better representation of the vegetation compared to a straight cylinder. Besides the representation of a cylinder as vegetation, a cylinder can also represent bridge piers, wind turbine foundations or other hydraulic structures in water.

1.2 Literature review

To understand the interaction between vegetation and flow, lab experiments and numerical modelling have been performed. First, there are studies that focus on large scale processes around dense vegetation. The dense vegetation can be modelled as rigid cylinders in a certain pattern. Baptist et al. (2007) formulated equations for the flow resistance caused by the vegetation. The equations are based on the characteristics of the vegetation and the bed. The flexibility of the vegetation is not taken into account and thus are the equations less suitable for flexible vegetation (Baptist et al., 2007). Nepf and Ghisalberti (2008) focusses on the turbulence structure, velocity profiles and dispersion of the flow for submerged vegetation in channels. They concluded that the turbulence was mainly generated by the shear-scale turbulence above the vegetation and the turbulence generated by the canopy. The vegetation also has a dampening effect on the waves, a combination with the critical wave velocity and the dampening led to the length where the sediment would be entrained within submerged vegetation (C. Tang et al., 2019). Besides these experimental results, also numerical simulations have been executed. King et al. (2012) focusses on improving a Reynolds Averaged Navier Stokes (RANS) $k-\epsilon$ model based on different length scales of the vegetation and channel, like water depth and plant height. Their motivation was to predict velocities, turbulent diffusivities and scalar dispersion for a specific vegetation specie. Etminan et al. (2018) increased the robustness of a bed shear stress model for flow within emergent vegetation. As the bed shear stress is highly variable around vegetation, the model improves the prediction of the average bed shear stress using a Large Eddy Simulation (LES) model. Instead of modelling cylinders, another option is to include the drag of the vegetation in the momentum equation. J. Tang et al. (2024) focused on the TKE generated in the water waves in the momentum equation. They concluded that the wave amplitude has a significant effect on the stem-generated turbulence. In the papers above, the focus was on the large structures caused by vegetation patches, where mainly the sweep and ejection events above the vegetation are modelled. Reducing the vegetation to a part of the momentum equation neglects the fact of the coherent structures caused by the vegetation. Furthermore, can there be learned, that for both emergent vegetation and submerged vegetation the turbulence generated by the cylinders are an important factor of the turbulence.

The interaction between the flow and a single cylinder already have a large impact on the flow and bed shear stress (Aksel et al., 2021; Chang & Constantinescu, 2023; Kirkil et al., 2008, e.g.). In Figure 1.1 can be seen that the flow upstream of the cylinder is bended downwards due to the vertical pressure gradient that is higher at the top. At the bottom a separation region is formed, in which a horseshoe vortex (HV) system is formed. The HV is advected with the flow. On the sides of the cylinder the streamlines of the flow contracts, leading to higher velocities at the sides. The contraction of the streamlines and HV leads to an increase in bed shear stress(e.g. Roulund et al., 2005). Due to the pressure gradient at the cylinder flow separation occurs, leading to a wake

behind the cylinder. In the wake regular lee-wake vortices are shed.

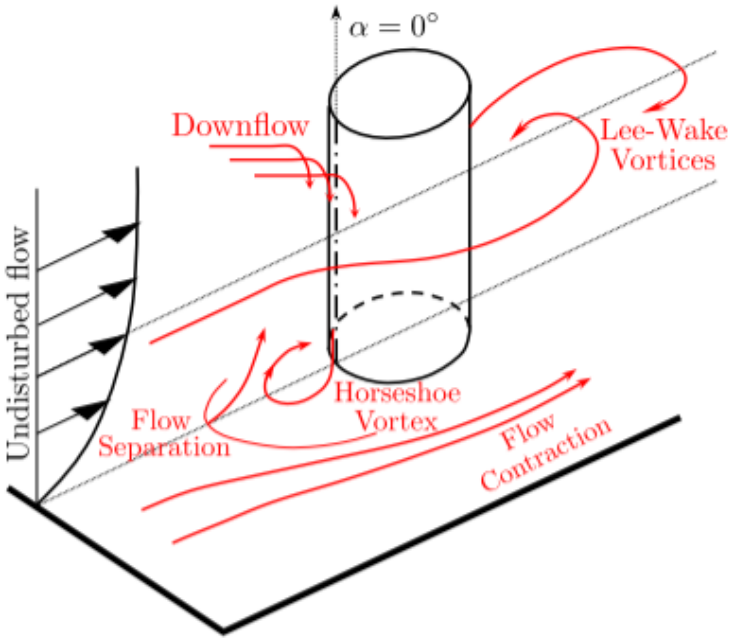

Figure 1.1: Sketch of flow around a straight cylinder from Kitsikoudis et al. (2017)

For example, Chang and Constantinescu (2023) focussed on a vertical cylinder in a flat bed with oscillatory flow, where the focus was mainly on the effects of changing the oscillation of the flow. They used Detached-Eddy Simulations (DES), LES and RANS simulations for their research. They also found that DES was the most accurate in predicting the turbulent parts. The RANS was able to capture the phase-averaged streamwise velocity, but the bed shear stress was not as accurate. The remark that DES is a good model for the turbulent structures, is supported by the simulations of Kirkil et al. (2008). Other papers focus on the scour around a vertical pile without waves (e.g.(Aksel et al., 2021; Baykal et al., 2015; Kirkil et al., 2008; Roulund et al., 2005)). Roulund et al. (2005) used a RANS $k-\omega$ model to investigate the scour around a cylinder. They investigated different Reynolds numbers and for different boundary layer thicknesses in relation to the pile diameter and roughness. Their research agreed well with the measured scour depth in experiments. Kirkil et al. (2008) found that the horseshoe vortex (HV) system consists of a primary necklace vortices with several other secondary vortices. These coherent structures were modelled using LES. Also Aksel et al. (2021) did a simulation of a vertical cylinder at a flat and scoured bed with a RANS $k-\omega$ model. Their conclusion was that due to the presence of the scour hole the lee-wake vortices significantly weakened. The scour hole resulted in the presence of large-scale counter-rotating streamwise vortices. Overall the scour hole seems to streamline the flow around the cylinder(Aksel et al., 2021). The coherent structures as the HV result in an increase in bed shear stress and in the end also scour. Baykal et al. (2015) focussed on predicting the scour around a cylinder using as well an $k-\omega$ model. They concluded that the vortex shedding has a limited effect on the scour process, where the main impact is to the early stages of the scouring process. This can also be contributed to the conclusion from Aksel et al. (2021) that the lee-wake vortices disappear and large-scale counter-rotating streamwise vortices are appearing(Baykal et al., 2015; Kirkil et al., 2008).

The inclined representation of a cylinder is important, because the bending has a large influence on the flow field (Kitsikoudis et al., 2017; Vargas-Luna et al., 2016). Less research has been done for inclined cylinders. In the paper of Kitsikoudis et al. (2017) the flow around an inclined cylinder is explained. There can be seen that due to the inclination the downflow in front of the cylinder has weakened, see Figure 1.2. The decrease in downflow results in a weaker HV and therefore also a smaller bed shear stress(?, ?). Furthermore can be seen that the shedding of vortices becomes more irregular and that now behind the cylinder upflow is present.

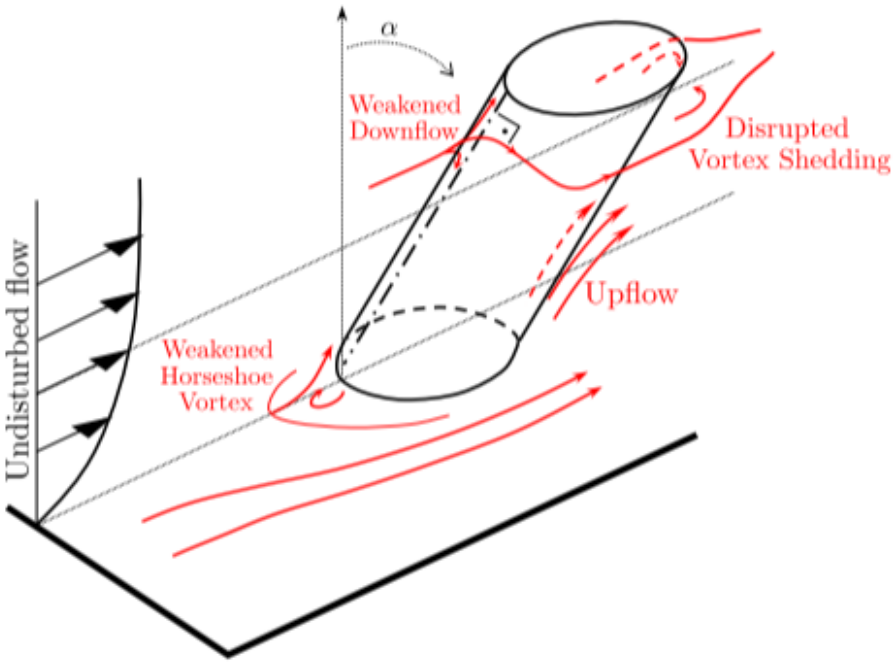

Figure 1.2: Sketch of flow around an inclined cylinder adapted from Kitsikoudis et al. (2017)

Far from the bed a cylinder in water can be considered as a infinitely long cylinder. For an infinitely long cylinder the flow crosses the cylinder perpendicular to the surface (Zhao et al., 2009). Additionally, with the Direct Numerical Simulation (DNS) was visible that the pressure difference between upstream and downstream of the cylinder decreased with increasing inclination angle. M. Liu et al. (2024) found that the vortex shedding frequency decreased for inclined cylinders, with even no vortex shedding for cylinder below 60°. They found that there was a large recirculation zone downstream of the cylinder for an inclination between 7.5° and 30° of inclination. Kitsikoudis et al. (2017) tested four different inclination angles in downstream direction to assess the velocity and the scour patterns. It was found that with inclination the upward velocity downstream of the pile increases as well as the fluctuations. Further, the results indicated that an inclined cylinder is more streamlined as the contraction of streamlines decreases and vortex shedding played less of a role for inclined cylinders. In addition, they found that the horseshoe vortex is weakened with increasing inclination angle. This also led to a decrease in scour depth and scour volume for inclined cylinders. With increasing inclination a the streamwise and transverse velocity fluctuations diminished, but the vertical turbulence played a larger role. Using these experiments, Aksel (2023) performed a numerical study with a $k-\omega$ model and concluded that the amplification of the bed shear stress

drastically decreased, which also supports the conclusion that the HV weakened. Additionally, the flow dynamics became more stable instead of cyclical. In the paper of Y. Liu et al. (2024) the main conclusion was that the due to the inclination angle the horseshoe vortex weakens, leading to a decrease in scour depth. Also in the scour simulations of Du et al. (2019) the scour depth decreased with increased inclination angle. Furthermore, it seems the contraction of the streamlines to have a big influence on the local scour.

1.3 Knowledge gap

From the literature on emergent and even sub-merged vegetation can be learned that the interaction between the flow and the cylinder is a very important cause of turbulence. As flexible vegetation bends with the flow, an inclined cylinder is likely more representative. From the studied literature we can see that the inclination alters the flow leading to a change in flow field and bed shear stress. This leads to the hypothesis that inclination is important in modelling vegetation. Therefore it will likely have a large effect on the flow. For the straight cylinder the scour hole has been extensively researched. From the impact of scour around a straight cylinder we can learn that also scour has an effect on the flow field. This yields two important factors for the simulating vegetation. For the inclined cylinder the literature covers the scour processes, but not the flow field and bed shear stresses if the scour hole is included.

1.4 Research questions

From the problem context, can be concluded that little is known about the effect of the scour hole on the flow field and bed shear stress for bent vegetation. The aim of this research is to understand the effect of inclination and scour of vegetation on the flow field and the bed shear stress. The vegetation is represented by a single cylinder, the inclination angle has a large influence on the flow field and bed shear stress(Aksel, 2023; Kitsikoudis et al., 2017). This aim results in a research question: "How does the bending of vegetation and scour of the bottom affect the flow structure and bed shear stress?". The main research question is supported by four sub questions:

1. How does a RANS-simulation that predicts the fluid dynamics around an inclined circular cylinder compare to experimental results?
2. How does the inclination of a cylinder affect the flow structure close to the cylinder and bed?
3. How does scour affect the flow structure around a straight and inclined circular cylinder?
4. How does scour and inclination affect the bed shear stress?

Depending on the water depth, there is submerged and emergent vegetation present in the salt marsh. There has been chosen to model emergent vegetation, as for both the stems are a major contributor to the turbulence. Moreover, only tide-dominant cases are considered, which result in that the waves are excluded. To simplify the tides only uni-directional flow is modelled. In terms of weather conditions the simulations will resemble more daily, calm weather conditions were the vegetation is not bended to moderate weather conditions were the vegetation is slightly

bended. Furthermore, this leads to the clear water scour that was also present in the experiments of Kitsikoudis et al. (2017). In the case of the emergent vegetation will be looked into the change in flow field and bed shear stresses. This problem can be modelled using RANS simulations. The RANS-modelling will decrease the accuracy compared to a DES or LES simulation, but decrease the computational time. Moreover, the RANS simulation has converges more easily as it has less grid restrictions. In addition is a RANS-simulation still able to solve large parts of the turbulence and is also often used in same cases (Aksel, 2023; Aksel et al., 2021; Baykal et al., 2015, e.g.) To answer the effect of inclination a cylinder with 0° and 14° are compared to each other, which can both be validated on the experiments of Kitsikoudis et al. (2017).

Chapter 2

Methodology

2.1 Overview of model components and simulations

In this chapter, the development of the models are described. First a general model concept will be introduced. The model concept consists of the model equations, mesh requirements, boundary conditions and initial conditions. These are for a large extent the same throughout all simulations. The differences between the models will be addressed in the section of each simulation. The lay-out of this chapter is visualized in Figure 2.1. Different models are generated to answer the main research question. To answer the effects of inclination 2 different inclination angles are chosen, which are 0° and 14°. Also scour has an effect on the flow field and bed shear stress, to understand this the cases have to be ran with and without a scoured bed. The 2 inclination angles and the option of scour and no scour leads to 4 cases in total. An overview of all the cases can be found in Table 2.1. For each case the initial conditions, boundary conditions made and the mesh has to be generated, as visualized in Figure 2.1.

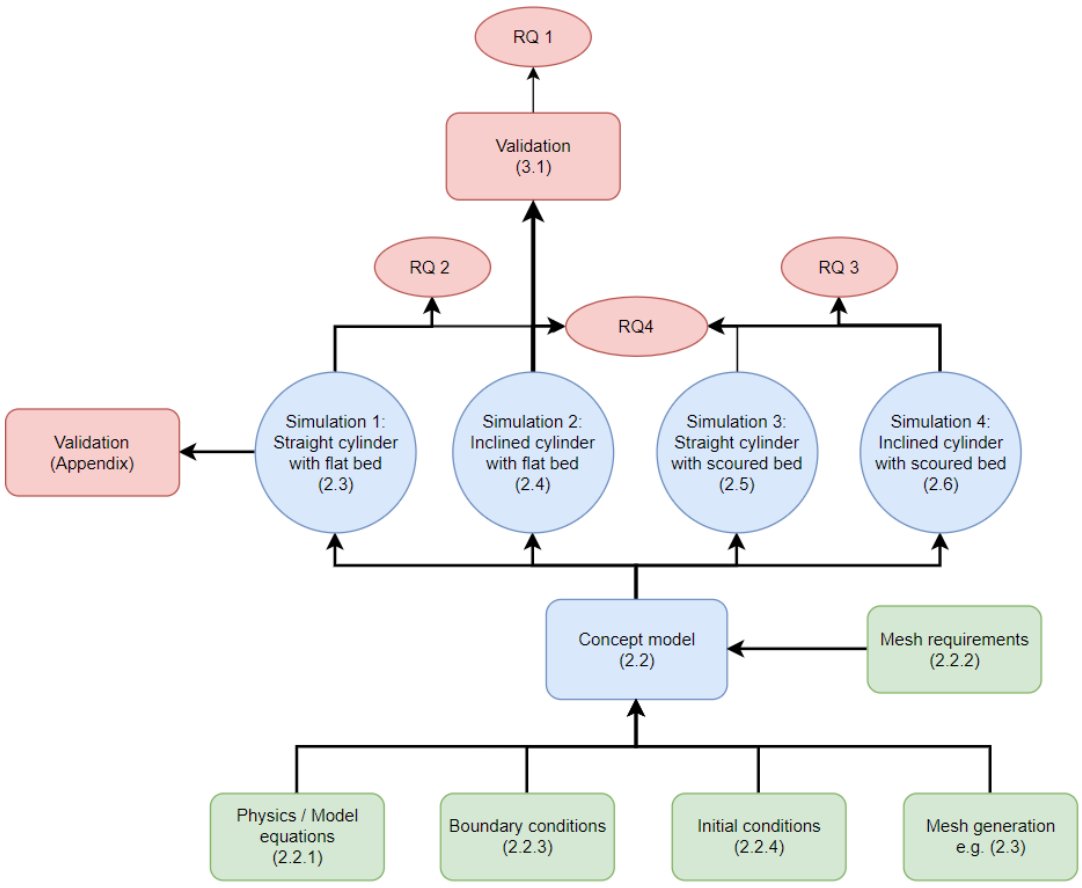

Figure 2.1: Structure of the methodology with the connections to each research question

		Inclination	
		0	14
Scour	No	Simulation 1	Simulation 2
	Yes	Simulation 3	Simulation 4

Table 2.1: Model simulations overview

To answer the research questions, different scenarios have to be modelled. To validate the models, the experimental results of Kitsikoudis et al. (2017) are compared to the numerical results of simulation 1 and 2. In order to answer RQ 1 simulation 2 needs to be compared. As simulation 1 is also validated, the results are included in the Appendix. The difference between simulation 1 and 2 is the inclination angle that changes from 0° to 14°. The effect of the inclination angle is covered in RQ 2, which will be answered using these two simulations. The difference between simulation 3 and 4 is also the inclination angle, but now also scour is included in the simulations. Hence, these Simulations 3 and 4 will be used to answer RQ 3. The implemented bed is the equilibrium scoured bed from Kitsikoudis et al. (2017). The last research question is about the bed shear stress. Answering RQ 4 requires the results of all 4 simulations.

2.2 Model concept

The modelled cases are flume experiments based on the set-up and scoured bed of Kitsikoudis et al. (2017). The concept is a cylinder inside a flume. The flow will become turbulent, caused by the cylinder. The turbulence in the flow is related to the Reynolds number. The Reynolds number is defined as $Re_D = U_0 D/\nu$, where U_0 is the depth average flow velocity and D is the cylinder diameter and ν is the viscosity of water. This leads to a Reynolds number of $Re \approx 2 \times 10^4$, which indicates transitional unsteady flow. Numerical modelling of such a problem requires Computational Fluid Dynamics (CFD) software. The open source software of OpenFOAM is often used for these kind of problems. OpenFOAM is able to model complex fluid flows with turbulence(OpenCFD Team & Nagy, 2025). Problems involving flow around a cylinder have been modelled before with OpenFOAM (e.g., Baykal et al., 2015; Y. Liu et al., 2024; J. Tang et al., 2024). The modelled fluid is water, so an incompressible solver is used. To model the transient behaviour of vortex shedding, the OpenFOAM solver pimpleFoam is used. The steady state solver simpleFoam is used, for the steady conditions of the inlet conditions. Both solvers are based on the finite volume options. For the stability of the model, a maximum Courant number is used. The Courant number is defined as $Co = \frac{u\Delta t}{\Delta x}$, which is a relation between the velocity (u), the timestep (Δt) and the size of a cell (Δx). For the current simulations a maximum Courant number of 0.7 is implemented. This means that a particle can travel a maximum of 0.7 cells at one timestep. Further, the model requires some spin-up time, which is set to 100 seconds after which is simulated until t = 150 seconds for the results. Resulting in 50 seconds of data. The number of cells is on the order of magnitude of millions, which require a lot of computational power. To minimize the calculation time, the simulations have been ran on Snellius. Snellius is a supercomputer in the Netherlands. A simulation ran for 100 seconds with 64 cores took around 40 hours of time. In the rest of this section the concept model is explained. The concept model consists of the model equations, boundary conditions and initial conditions.

2.2.1 Model equations

Certain equations have to be calculated in order to solve the dynamics of the flow. In this section, the model equations for the RANS simulations will be explained. All the model equations are the same for the 4 simulations. The numerical model in OpenFOAM solves a time-averaged version of the Navier-Stokes Equations. The modelled fluid in this case is water, which is incompressible. Therefore the incompressible Navier-Stokes equation are applied, which is described by Equation 2.1 (in Einstein summation convention). In this equation u is the velocity, t is the time, x denotes the Cartesian coordinate, g is the gravitational force, ρ is the density of the fluid and p is the pressure. The units of all the parameters can be found in the List of Parameters. The first term of the momentum equation is the inertia of the water and the second part is the convective acceleration. The first term on the right hand side is the gravitational force, where the second term is the pressure force and the last term represents the viscous forces on the fluid.

$$\frac{\partial u_i}{\partial t} + u_k \frac{\partial u_i}{\partial x_k} = g_i - \frac{1}{\rho}\frac{\partial p}{\partial x_i} + \nu \frac{\partial^2 u_i}{\partial x_j \partial x_j} \tag{2.1}$$

The momentum equation is combined with the continuity equation, see Equation 2.2.

$$\frac{\partial u_i}{\partial x_j} = 0 \tag{2.2}$$

The velocity changes a lot over time and is decomposed into an average velocity ($\overline{u_i}$) and a fluctuation of the velocity (u_i'), see also Equation 2.3. The decomposition of the velocity according to Equation 2.3 is also called Reynolds decomposition.

$$u_i = \overline{u_i} + u_i' \tag{2.3}$$

Using the method of Reynolds decomposition, the momentum equation is rewritten into Equation 2.4. Equation 2.4 is also called the incompressible Reynolds-Averaged Navier-Stokes (RANS) equations, in which S_{ij} is the mean-strain-rate tensor and τ_{ij} is the Reynolds stress tensor. Compared to Equation 2.1 the velocities are averaged and an extra term is added. The added term is the Reynolds-stress tensor which adds the effect of the turbulent motion on the time-average stresses.

$$\frac{\partial \overline{u_i}}{\partial t} + \overline{u_j}\frac{\partial \overline{u_i}}{\partial x_j} = -\frac{1}{\rho}\frac{\partial \overline{p}}{\partial x_i} + \frac{\partial}{\partial x_j}(2\upsilon S_{ij} + \frac{\tau_{ij}}{\rho}) \tag{2.4}$$

The fourth fraction of Equation 2.4 is the mean strain-rate tensor which is expressed by Equation 2.5.

$$S_{ij} = \frac{1}{2}(\frac{\partial u_i}{\partial x_j} + \frac{\partial u_j}{\partial x_i}) \tag{2.5}$$

The last part in Equation 2.4 is the Reynolds stress tensor, which is rewritten as Equation 2.6 based on the Boussinesq approximation. δ_{ij} is the Kronecker delta, ν_t is the eddy viscosity and k is the turbulent kinetic energy density

$$\frac{\tau_{ij}}{\rho} = -\overline{u_i' u_j'} = 2\upsilon_t S_{ij} - \frac{2}{3}k\delta_{ij} \tag{2.6}$$

$$k = \frac{1}{2}\overline{u_i' u_j'} \tag{2.7}$$

To make sure that the model is able to solve the equations a turbulence closure model needs to be used. The $k-\omega$SST model is chosen to model the turbulence as this model predicts the best adverse pressure gradients (Menter, 1993). In this model the $k-\epsilon$ model is used in the free-stream, so far from the walls as it is less accurate for cylinders (King et al., 2012). Closer to the walls, the model uses the $k-\omega$ closure model. These two equations for k and ω are expressed in Equation 2.8 and 2.9.

$$\frac{\partial k}{\partial t}+u_j\frac{\partial k}{\partial x_j}=\frac{\partial}{\partial x_j}[(\mu+\sigma_k\nu_t)\frac{\partial k}{\partial x_j}]+\frac{\tau_{ij}}{\rho}\frac{\partial u_i}{\partial x_j}-\beta^* k\omega \tag{2.8}$$

$$\frac{\partial \omega}{\partial t}+u_j\frac{\partial \omega}{\partial x_j}=\frac{\partial}{\partial x_j}[(\mu+\sigma_\omega\nu_t)\frac{\partial \omega}{\partial x_j}]+\frac{\gamma}{v_T}\frac{\tau_{ij}}{\rho}\frac{\partial U_i}{\partial x_j}-\beta\rho\omega^2+2\rho(1-F_1)\frac{\sigma_{\omega 2}}{\omega}\frac{\partial k}{\partial x_j}\frac{\partial \omega}{\partial x_j} \tag{2.9}$$

The first term in Equation 2.8 (Menter, 1993) and 2.9 (Menter, 1993)is the temporal part. The second term is the advective part of the equation and the third term is the dispersion of the turbulence. The fourth part is the production term and the fifth term is the dissipation term. The sixth term is only present in Equation 2.9 where it represents the diffusion between k and ω. These two equations are specific for the $k-\omega SST$ model. These calculations do not solve for the turbulence, but the equations model the turbulent kinetic energy within a cell in the parameter k. This means the result will always contain an error (Spalart, 2009), but decrease the computational time a lot (Chang & Constantinescu, 2023; Spalart, 2009). Solving the time-averaged Navier-stokes equation and the continuity equation gives the results presented in the next chapter.
In order to solve the equations for all parameters in a numerical way. Schemes for time and space have to be used. For k,ω,ν_t,u a bounded Gauss Linear upwind is used. To ensure stability, the backward Euler scheme is used in the model (*OpenFOAM The Open Source CFD Toolbox User Guide*, 2024; Wilcox, 2010). Furthermore, a linear interpolation scheme is used. Last for the calculation the walldistance the Meshwave method is used (OpenCFD Team & Nagy, 2025).

2.2.2 Mesh requirements

To generate the grid OpenFOAM provides two options for grid generation. These are blockMesh and snappyHexMesh. The benefit of a blockMesh model is the easy adjustment of locations, the smooth grading and the fast generation of a mesh. The downside is that the grading for a cylindrical part is harder, further is the curvature in the model visible over a longer distance, which also can lead to numerical diffusion. The last downside is that irregular surfaces or complex shapes are hard to model, due to the increase in the number of blocks. The other mesh generator from OpenFoam is snappyHexMesh. The snappyHexMesh model uses a 1:2 refinement between different refinement levels. This means that if level 0 consists of cells that are 4 mm wide, than level 1 has 2 mm cell sizes. This allows fast refinement near important areas. However, this also induces a numerical diffusion as the transition is not very smooth as with blockMesh. The benefit of snappyHexMesh is that complex geometries can be used to generate a mesh, this is especially useful for simulation 3 and 4 where a scour hole is included. This comes at the cost that if the number of cells are increased the mesh generation takes much longer than blockMesh. Another benefit is the ability to add layers close to the patches. This is necessary for the refinement near the walls. Close to the wall the tangential flow speed increases very fast, because there is the transition between the no-slip condition of the wall and the free stream far away of the wall. For high Reynolds numbers the velocity profile is sketched as in Figure 2.2 (Greenshields & Weller, 2022).

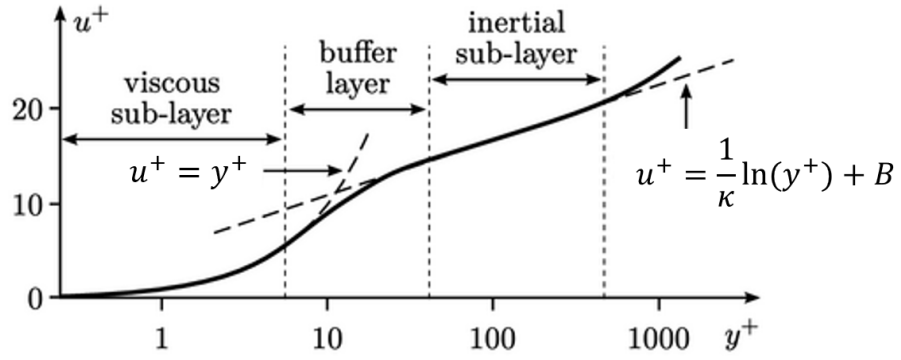

Figure 2.2: Relation between the dimensionless velocity and wall distance adapted from Greenshields and Weller (2022)

The dimensionless velocity (u^+) is formulated as $u^+ = u/u_\tau$, where u is the streamwise velocity and u_τ is the friction velocity. The dimensionless wall distance (y^+) is formulated as $y^+ = u_\tau y/\nu$, where u_τ is the friction velocity, y is the distance to the wall and ν is the viscosity of the water. The reason to model until the viscous sublayer is that the equations in the buffer layer are less accurate, see Figure 2.2. Reducing the dimensionless wall distance below 5 results in a more accurate estimation of the bed and/or wall shear stresses (Greenshields & Weller, 2022). But there is a trade-off between accuracy and the computational time. As more cells mean more computation time. To make the trade-off between accuracy and computational time, there is chosen to have an average y^+ of around 5 and maximum of 10 as the behaviour of the parameters is still quite linear in those regions, see Figure 2.2.

The requirement in mesh size is the first important requirement, but there are more mesh requirements. snappyHexMesh generates a mesh based on several other requirements. These requirements are for example the orthogonality, minimal volume or the skewness of the cells. The values chosen are the standard values from an OpenFOAM tutorial and the slides of Guerrero (2021). The values can be seen in Table B.1 in Appendix B. OpenFOAM also has the utility to check the mesh based on the mesh requirements, which is called checkMesh. This option checks if all the boundaries are defined and other mesh requirements, for example the aspect ratio, minimum volume and non-orthogonality. This is very useful for mesh generated with blockMesh as it has not a mesh requirement check in the generation process. The meshes for each simulation passed the checkMesh test of OpenFOAM.

2.2.3 Boundary conditions

In this section the boundary conditions will be described for the model concept in Table 2.1. The cases resemble a cylinder in a flume with a bed. To match the experimental set-up for validation the side boundaries have been modelled as walls, as are the bottom and the cylinder, see also 2.3. The top of the flume will be modelled as a rigid-lid. This means that the change in surface elevation is negligible (Baykal et al., 2015). This assumption is valid based on the Froude number given by Equation 2.10 in which u is the undisturbed free stream velocity, g is the gravitational force and h is the water depth of the simulation. The Froude number for the simulation is 0.12, which is below the 0.2 and thus a rigid-lid assumption is applicable. In OpenFOAM a rigid-lid can be modelled as

a symmetry plane, see Figure 2.3. As there are no restrictions for velocity components u and v, but $w = 0$. So there is no flux outside of the domain, which is physically the same as a rigid-lid.

$$Fr = \frac{u}{\sqrt{gh}} \tag{2.10}$$

In Figure 2.3 the boundary conditions of the simulation are visualized. The functions are defined in the first timestep in OpenFOAM for each of the patches.

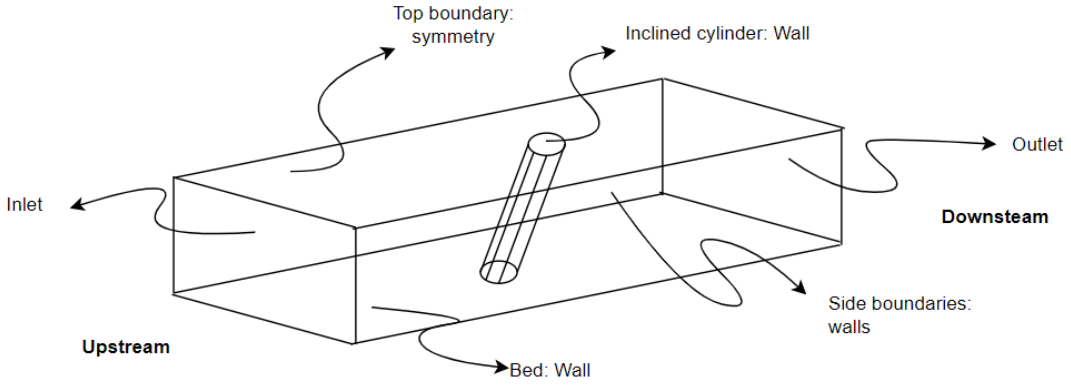

Figure 2.3: A conceptual overview of the boundary conditions for each patch defined in OpenFOAM. All the boundaries enclose the internal field.

An overview of these functions is shown in Table 2.2. For the bottom and cylinder functions that are able to resolve the boundary layer are used (Guerrero, 2021). As the side walls are not refined, wallfunctions are sufficient for the simulation. For the velocity at the outlet the OpenFOAM function PressureInletOutletVelocity is used, which is a zero gradient boundary condition for outflowing water. For inflowing water, it assigns a fixed velocity (OpenCFD Team & Nagy, 2025). The velocity is set to 0 in all directions, as this will not disturb the solution. There is no indication that there is an inward flux at the outlet of the domain during the simulations. For the k and ω the OpenFOAM function inletOutlet is used, which also applies a zero gradient condition for inflowing flow and a fixed velocity if there is inflow (OpenCFD Team & Nagy, 2025). For the eddy viscosity ν_t a calculated boundary condition is applied which is the same as the internal field.

Variable	**Cylinder and bottom**	**Walls**	**Top**	**Outlet**	**Inlet**
U	No slip	No slip	SymmetryPlane	PressureInletOutletVelocity	Initial Conditions
p	ZeroGradient	ZeroGradient	SymmetryPlane	FixedValue	ZeroGradient
k	kLowReWallFunction	kqRWallFunction	SymmetryPlane	inletOutlet	Initial Conditions
ω	FixedValue of 10	FixedValue of 10	SymmetryPlane	inletOutlet	Initial Conditions
ν_t	FixedValue of 0	nutkWallFunction	SymmetryPlane	calculated	Initial Conditions

Table 2.2: Overview of functions for each patch

An overview of the different conditions that have been assigned to each patch is shown in Table 2.2. Some of them are called wall functions. OpenFOAM gives the option to model parameters using wall functions close to the wall. The wall functions blend a parameter based on a certain equation. Some wall functions take the wall distance into account, for example omegaWallFunction or kLowReWallFunction, others like the kqrWallFunction does not take the wall distance into account and is just a simple wrap around a zero gradient boundary condition (OpenCFD Team &

Nagy, 2025). Only wall functions in OpenFOAM is not sufficient, also values have to be assigned to these wallfunctions and other boundary conditions. Namely for the pressure at the outlet, which is 0. But also for k, which should be a very low number near the wall, chosen is a number 100 times smaller than the calculated k in Equation 2.13. Physically, k has to be 0 as there are no fluctuations in the flow velocity at the wall, but the numerical model crashes for a value of 0. For ω (energy dissipation) a high value should be used to model the energy dissipation at the wall (Guerrero, 2021). This means from a physical perspective that the wall is dissipating a lot of energy. In Equation 2.11 (Guerrero, 2021), in which ω_{wall} the specific dissipation rate at the wall, Δy the distance from the cell at the wall to the wall itself, β_1 is a model parameter and ν is the kinematic viscosity of water. The equation leads to a value 12800 for the specific dissipation rate at the wall.

$$\omega_{wall} = (10)\frac{6v}{\beta_1(\Delta y)^2} \tag{2.11}$$

2.2.4 Initial conditions

To achieve realistic results the flow at the inlet should be fully developed. A fully developed flow is achieved when the water flows through an empty flume with the same water depth (0.30 m) and width (0.98 cm), so without a cylinder inside the flume. The total length of the flume is extended to 50D, where D is the Diameter of the cylinder. A fully developed flow is characterized by a logarithmic velocity profile along the depth and a linear bed shear stress at the bottom and walls over the depth in the viscous sublayer. At the inlet of the empty flume an uniform velocity of 0.214 m/s is fixed, which is the same as the depth-average velocity (u_0). The velocity develops over distance towards a logarithmic profile, as is visible in Figure 2.4. At the outlet the data is extracted per cell, which will be used as initial conditions (IC) for the simulation. The same grid-sizes and locations of the cells are required for the IC and the inlet of the simulation, because the output of the IC is directly implemented as the input at the inlet.
To execute the run for the IC of the final mesh, the boundary conditions have been defined based on section 2.2.3. The boundary conditions enclose the simulation, but the internal field needs initial values. These initial values are k, ν_t and ω.

$$I = 0.16Re^{-\frac{1}{3}} \tag{2.12}$$

The initial value of each parameter is chosen based on several formulas. The first step is to calculate turbulence intensity (I) based on the Reynolds number (Re), see equation 2.12 (Aksel, 2023). The turbulence intensity is $0.16 \cdot 2 \cdot 10^4 = 0.32 \cdot 10^4$.

$$k = \frac{3}{2}(u_0 I)^2 \tag{2.13}$$

The turbulence intensity is then used to calculate turbulent kinetic energy with the free stream depth-averaged velocity (u_0), see 2.13 (ANSYS Inc, 2009). This results in a value of $\frac{3}{2} \cdot (0.214 \cdot 0.046)^2 = 1.2 \cdot 10^{-5} m^2/s^2$.

$$l = 0.07D \tag{2.14}$$

To calculate omega (ω), first epsilon (ϵ) and the turbulent length scale have to be calculated. Turbulent length scale (l) is dependent on the diameter of the cylinder (D), see 2.14 (ANSYS Inc, 2009). The turbulent length scale is $0.07 \cdot 0.09 = 0.0063m$

$$\epsilon = c_{\mu}^{\frac{3}{4}} k^{\frac{3}{2}} l^{-1} \tag{2.15}$$

The next step is to calculate (ϵ), which is also used in the RANS $k - \epsilon$ model. In this equation, the c_{μ} is a model coefficient, which is standard set to 0.09 (Wilcox, 2010). This leads to a value of $0.09^{\frac{3}{4}} k^{\frac{3}{2}} l^{-1} = 4.69 \cdot 10^{-5} m^2/s^3$, see Equation 2.15 (ANSYS Inc, 2009).

$$\omega = \frac{\epsilon}{\beta^* k} \tag{2.16}$$

For the free stream value of ω, Equation 2.16 can be used. Filling in Equation 2.16 leads to a value of $0.317 s^{-1}$, which is also within the limits set in Menter (1993). To achieve that ω is between the limits β^* set to 1 instead of 0.09 which was given by (Wilcox, 2010).

$$\nu_t = \frac{k}{\omega} \tag{2.17}$$

The last parameter for the free stream is the turbulent or eddy viscosity (ν_t), which can be calculated using Equation 2.17, which resulted in a value of $4.66 * 10^{-4} m^2/s^2$.

When all the parameters are known, the IC-simulation can be ran for the specific simulation. In OpenFOAM the solver simpleFoam is used for this. This solver is able to solve steady states, which flow through a flume is for RANS-simulations. An overview of the IC can be seen in Figure 2.4, which are measured at the outlet of the IC. In Figure 2.4d the logarithmic profiles of the velocity can be seen for the different simulations. In the next Figure 2.4b the bed shear stress is shown. Simulation 2 shows a slightly different pattern, as only the first 4 points are linear, as these are in the viscous region with linear velocity. The other 2 points are within the buffer layer as the y^+ is above 5. The difference in the thickness of the viscous layer is related to the variable ω. ω has a logarithmic profile for the different simulations, see Figure 2.4e. It looks like that for the scour simulations the ω stops at 4000, however, that is due to the fact that the bottom itself is not included in the plot, as this is also not included in the file for the initial conditions, where only the cell centres are given. Due to the fact that simulation 2 has a smaller value for the omega, the energy dissipation is lower, resulting in a smaller viscous sublayer. Therefore the bed shear stress is logarithmic after 0.35 mm from the bed. For the model parameter k the fluctuations are the highest just outside the viscous sublayer. In side the viscous sublayer the fluctuations decrease again. The same holds for the eddy viscosity, which is the highest in the water column, but decreases to 0 at the wall. The initial conditions will be further discussed in the discussion as no validation or sensitivity analysis is done based on the parameters.

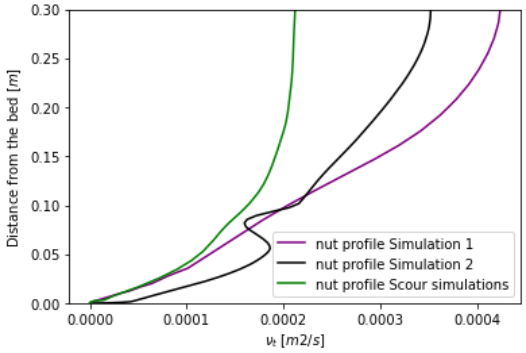

(a) Eddy viscosity ν_t. The fluctuation in simulation 2 is discussed in the Discussion.

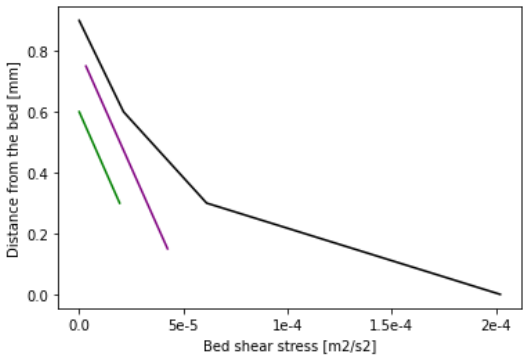

(b) Bed shear stresses τ

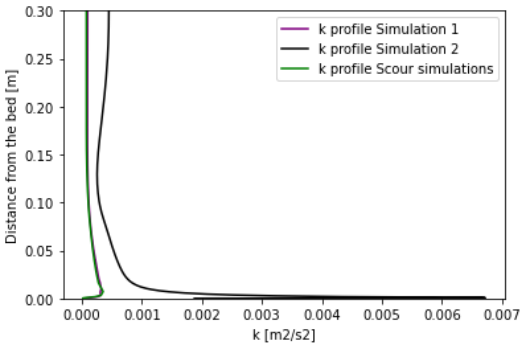

(c) turbulent kinetic energy k

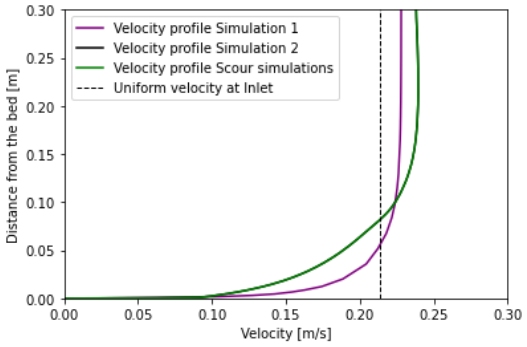

(d) Velocity U

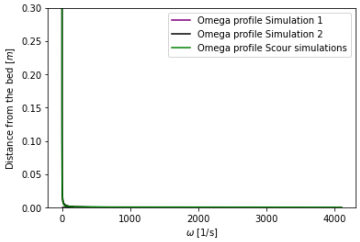

(e) Energy dissipation ω. For simulation 2,3,4 the bottom is not extracted from ParaView. Therefore the lines are shorter and the maximum specific dissipation rate is at 4000 $1/s$.

Figure 2.4: Values for the Initial Conditions at the inlet.

2.3 Simulation 1: Straight cylinder with flat bed

In Simulation 1 the general model equations, boundary conditions and initial conditions are applied. But the mesh generation is slightly different compared to the other simulations. The domain of the mesh is based on the experimental set-up used by Kitsikoudis et al. (2017). This means that several dimensions are fixed. The width of the domain is set to 0.98 m and the water depth to 0.30 m. Furthermore, the diameter of the cylinder is fixed to 9 cm. The centre of the cylinder is placed in the flume at x = 0 and y = 0, see Figure 2.5. For the comparison to the experiments later, the centre of the cylinder is shifted to x = -0.5D, y = 0 in dimensionless coordinates as this coordinate

system has also been used. The front of the computational domain is set to 0.45 m or 5D in front of the cylinder. Based on other numerical models the end of the model is set to x = 20D to make sure that the outlet is not influencing the results. The length makes sure that no large gradients in the parameters are interfering with the BC of zero gradient at the outlet.

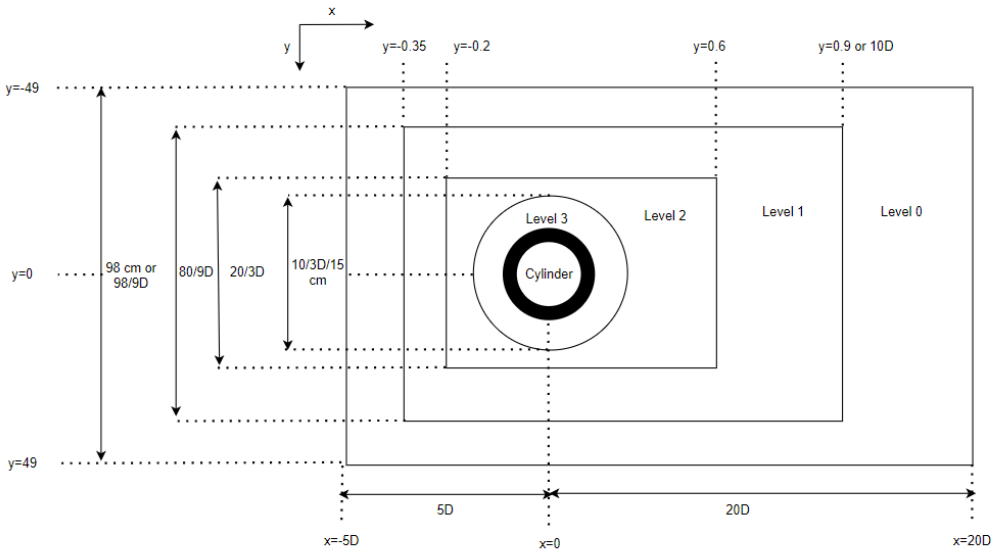

Figure 2.5: Topview lay-out for snappyHexMesh (not to scale)

The mesh is generated using snappyHexMesh. Where the grid is refined near the cylinder and bottom as these are the most important areas. Another region of interest is the wake of the cylinder. This area is important as this can be compared to the experimental results and the turbulence is the most present there. The refinement levels range from 0 to 3 and are 1.6-0.8-0.4-0.2 mm thick respectively. The cells are all cubic with a 1:1:1 ratio in x:y:z to increase the speed to add layers as well as the amount of added layers. To have a good coverage of the bottom and cylinder there are 4 layers of cells close to the patches added. Because in the case of more layers, the layers would collapse, which lead to increased y_+ values and irregular shaped cells. Without the added cells, the refinement is not sufficient to reduce the average y_+ below 5 as well as that the pressure distribution has large gradients near the cylinder. The 4 added layers are added close to the bottom and cylinder with an expansion ratio of 1.2 and the final layer thickness is 1.4 mm. The total thickness of the 4 layers is 4.3 mm thick. In the end the model consists of 10 million cells with an average y^+ of 4 for the bottom and 6 for the cylinder. In this case the maximum y^+ is 10 for the bottom and 11 for the cylinder.

2.4 Simulation 2: Inclined cylinder with flat bed

The second simulation is with a flat bed and an inclined cylinder of 14 degrees. The same model equations have been used for modelling the second simulation, see Section 2.2.1. In this simulation a blockMesh model is used, to get rid of the large refinement steps in snappyHexMesh. A blockMesh model contains different blocks, see Figure 2.6. Each row and column can be graded to get refinement

near important areas. Therefore the grading is such positioned that the cells are finer near the cylinder and bottom. Around the cylinder a circular refinement is used to get the cells aligned with the cylinder for a smoother pressure distribution, see Figure 2.6a. As the cells in B2-5 etc. are curved around the cylinder a rectangle is placed, so that the cells in row A,F and column 1 and 6 are not curved. The mesh is graded such that the transition between the different blocks are smooth from a visual perspective. Due to the inclination there is focused to have a smooth transition at the bottom. In general can be said, if the transition is hardly visible, then the mesh is graded well. The layout visualized in Figure 2.6a is generated for 3 different levels. At the bottom, at 2 cm from the bottom and at the water surface. The layer in between is chosen to handle more easily the refinement near the bottom. The coordinates $x2$, $x3$, $x4$, $x5$ and $x6$ shift due to the inclination of the cylinder, see Figure 2.6b.

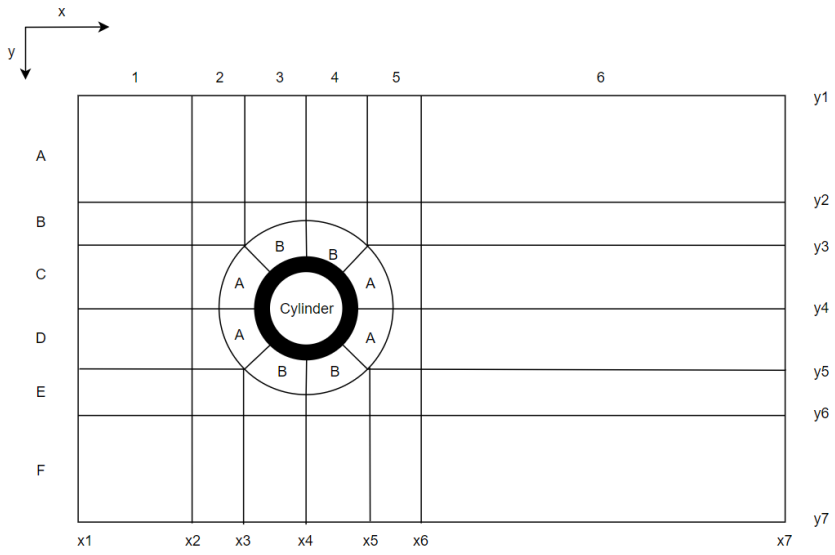

(a) Topview blockMesh model (not to scale)

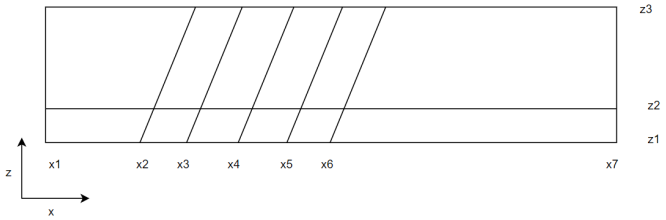

(b) Sideview blockMesh model (not to scale)

Figure 2.6: Overview blockMesh model for simulation 2

To get the same results the same coordinates have to be known, which are given in Table 2.3. The dimensions of the total domain are the same compared to the mesh in Section 2.3. The width of the refined cylinder is 9 cm. This means that for example $x3$ and $y5$ are at 45 degrees from the refinement around the cylinder. The circular part with all blocks A and B is needed to have the cells aligned with the cylinder for the pressure distribution.
Compared to Simulation 1 the BC have slightly changed. Instead of a value for omega of 10000 a value of 10 is used, which would lead to less energy dissipation at the walls, see Section 2.2.4. The cell size near the bottom is larger than for Simulation 1, 3 and 4, which would also imply that a

Parameter	x1	x2	x3	x4	x5	x6	x7	y1	y2	y3	y4	y5	y6	y7	z1	z2	z3
Value (cm)	-45	-30	$-9\sqrt{2}$	0	$9\sqrt{2}$	30	180	-49	-30	$-9\sqrt{2}$	0	$9\sqrt{2}$	30	49	0	2	30

Table 2.3: Coordinates of z1 (bottom layer) for the blockMesh model

smaller value can be used. For the blockMesh model the size of the cells cannot be calculated as it is unclear how large the distance from the cell centre to the boundary is. The rest of the boundary conditions can be found in section 2.2.3. As the mesh has now changed, the IC have to be ran again, but now with a blockMesh model. This is necessary to have the same amount and location of cells at the inlet for the final mesh. The values are the same as in Section 2.2.4. The final mesh has 5.1 million cells and an average y^+ at the cylinder of 6 and at the bottom of 4. The maximum dimensionless wall distance at the bottom is 10.6 and at the cylinder 11.42. The slightly higher wall distance at the cylinder is not a problem, as the shear stresses at the cylinder are not computed.

2.5 Simulation 3: Straight cylinder with scoured bed

The addition of the scour hole is the next step after the runs with the flat bed. The eroded bed of the experiments of Kitsikoudis et al. (2017) is used for the modelling. As the data is provided as point data in x,y and z, the data has to be transformed. The point data cannot directly be implemented in snappyHexMesh. To get the scoured bed in an stl-file that is suited for snappyHexMesh several iterations have been made. The next step is to get the undisturbed bed in front of the cylinder to z=0. However, the depth deviated in the order of magnitude of mm. Therefore an average depth is subtracted from the data. The data points at the inlet were slightly curved, which made it impossible to get good IC. Therefore is the inlet extended with 5 cm to have the whole inlet started at z = 0 and to make sure that for the initial conditions no transverse flow are present. The data points in between are linearly interpolated to have a smooth transition. The outlet is at 120 cm behind the centre of the cylinder, because the scoured bed ended around 120 cm. The generated coordinates have been loaded into Meshlab. Meshlab is a free software that is mainly used for 3D drawing. In Meshlab the normals have been calculated based on 15 neighbours and 1 smoothing iteration has taken place. After the normal calculation an surface reconstruction is made based on the screened poisson method from Kazhdan and Hoppe (2013). The result of a Digital Elevation Model (DEM) can be seen in Figure 2.7. The cylinder is slightly higher than 30 cm and lower than the scoured bed to make sure that the cylinder fully intersects the top and bottom of the mesh. This is not causing problems as the blockMesh that intersects the stl-file is set from $y = -0.49$m to 0.49m and thus are these sides outside of the mesh.

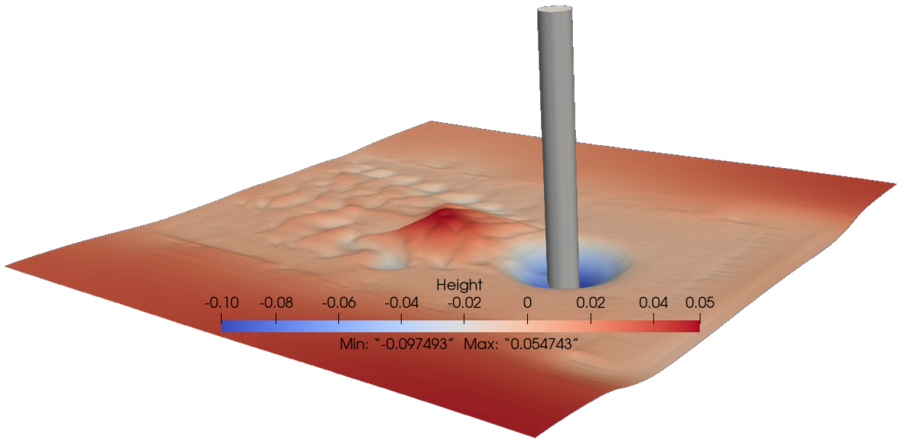

Figure 2.7: Digital Elevation Map (DEM) of Simulation 3

With the domain now fixed, the mesh is made. There is chosen to have 3 levels of refinement. With refinement levels changing from 9-4.5-2.25 mm in grid size. The level 3 (2.25 mm) refinement has a diameter of 2D, which almost fully covers the main scour hole. The level 2 refinement is set for z below 8 cm, so that it covers the whole scoured bottom, where a maximum height of around 6 cm is reached.

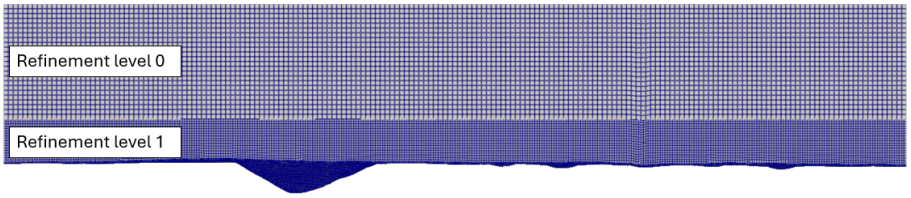

(a) Sideview

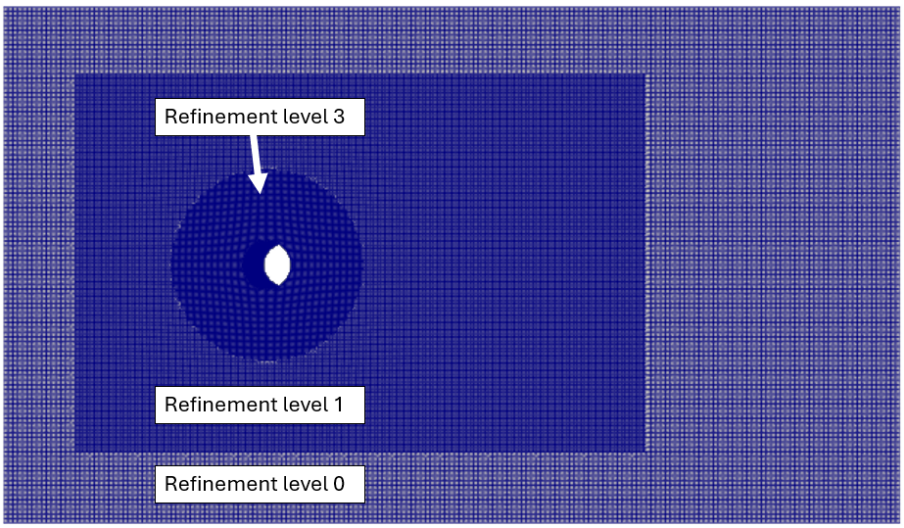

(b) Topview

Figure 2.8: Mesh used for the calculation of the hydrodynamics around a scoured inclined cylinder

Furthermore, a box refinement is created around the cylinder. The refinement box starts 4D (36 cm)

(from the cylinder centre) in front of the cylinder and ends 8D (72 cm) behind the cylinder and has a width of 4D (36 cm) to either side. SnappyHexMesh intersects the stl-files with the blockMesh set up before. After that only small layers have to be added to the mesh. Some iterations have taken place and the best results were achieved with 5 layers, with a expansion ratio of 1.1. This means that the total layer of added layers is 3.05 mm thick. The addition of these layers is to improve the alignment of the cells to the curvature of the cylinder and scour hole. This helps with the pressure distribution and to align the flow with the bed and to make sure that the y^+ is below 5. In the final mesh 99.2% of the bottom and 97% of the cylinder is covered with 5 layers of cells. Small parts at the bottom with a lot of curvature are not completely covered with the added cells. For the cylinder it is mainly at the connection with the scoured bed, see Figure 2.9.

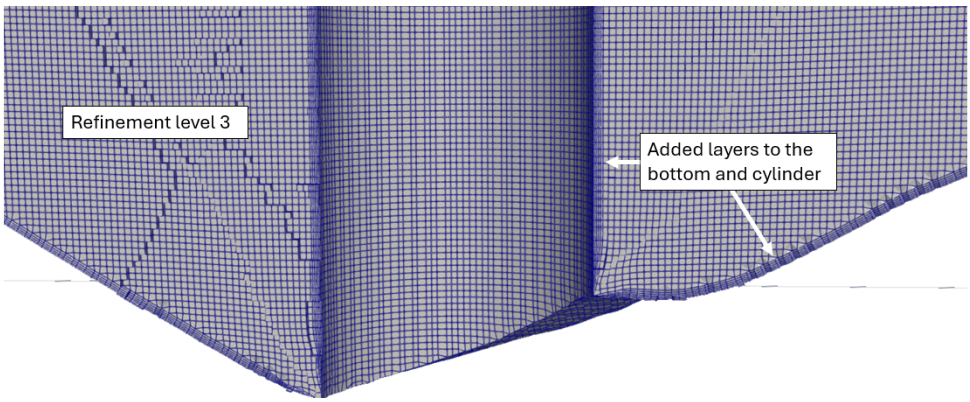

Figure 2.9: Connection between scoured bed and cylinder at the symmetry plane

The mesh generation leads to a mesh with 6.7 million cells. The average y^+ is between 2 and 3 for the bottom. But locally the increase in y^+ is 12. This is caused by the failure of the layer addition far from the cylinder.

2.6 Simulation 4: Inclined cylinder with scoured bed

The last simulation is the simulation of a scoured bed with an inclined cylinder of 14 degrees. Only the scoured bed and the cylinder have changed compared to simulation 3 in Section 2.5. During the mesh generation was found that the centre of the cylinder was not exactly at $x = 0$, so the centre of the cylinder is 4 cm moved in downstream direction for the final mesh. The scoured bed from Kitsikoudis et al. (2017) is shown together with the inclined cylinder in Figure 2.10.

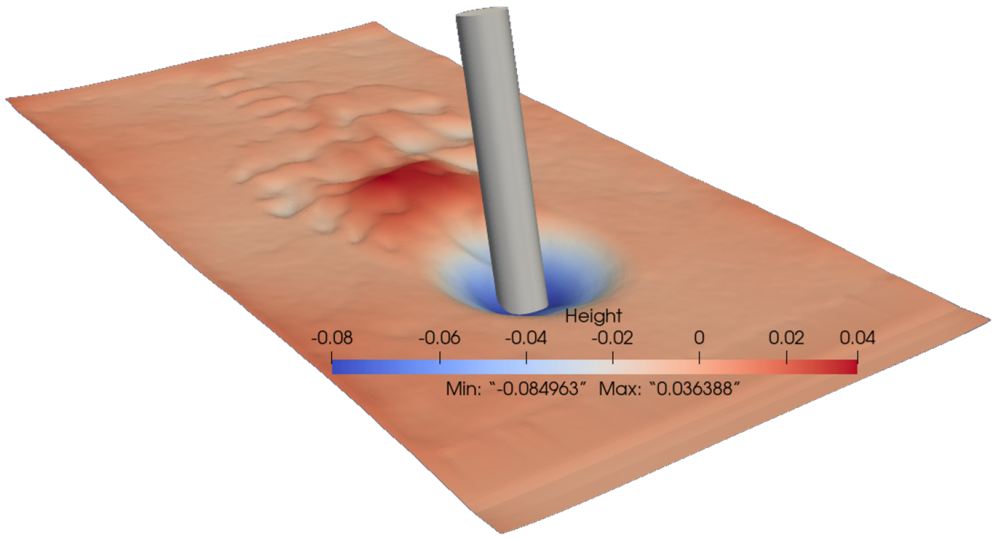

Figure 2.10: Digital Elevation Map (DEM) of Simulation 4

The mesh generation lead to a mesh with 6.7 million cells. The average y^+ is between 2 and 3 for the bottom. But locally the increase in y^+ is 12. This is caused by the failure of the layer addition far from the cylinder. Instantaneous y^+ can also be seen in Figure 2.11. There is visible that the largest part is below 6 and the every location close to the cylinder is below 10.

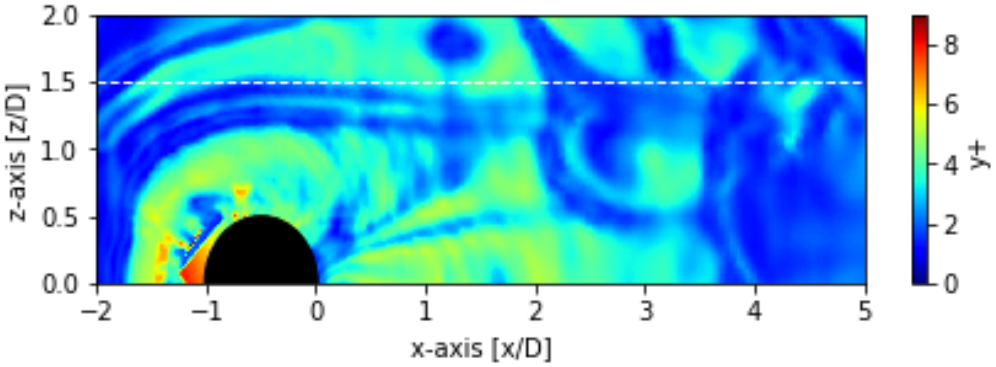

Figure 2.11: Instantaneous dimensionless wall distance around the cylinder. The black circle is the cylinder

2.7 Data extraction

After the simulations on Snellius in OpenFOAM-v2206, the next step is to extract the necessary data to answer the research questions. To decrease calculation time in python and decrease memory usage, 3 fields have been extracted, namely the bottom, at $z/h = 0.65$ and the symmetry plane (or $y = 0$), see also Figure 2.12. The bottom is used to visualize the bed shear stress. The symmetry plane is visualized to see the effect of the bottom and cylinder across the depth. The last field at $z/h = 0.65$ is far from the bed, so the influence of the bed is negligible and interesting to study. Further can these last two planes be compared to the experimental results of Kitsikoudis et al. (2017). These fields have been time-averaged (e.g. $\overline{u}$) and the fluctuations as root-mean-square (e.g. $u_{rms} = \sqrt{\overline{u'^2}}$ have been calculated for the parameters, but also the turbulent kinetic energy (TKE) is calculated, see Equation 2.7.

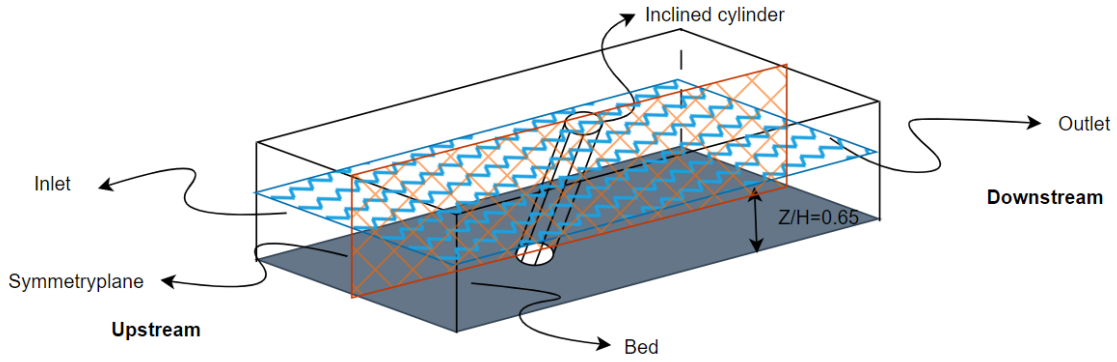

Figure 2.12: Planes extracted for post-processing

In Section 2.2.1 is mentioned that the RANS model is not able to capture all the turbulence. In the $k - \omega SST$ the turbulent kinetic energy within a computational cell is modelled in k.

$$TKE = k_{model} + \frac{1}{2}\overline{u_i' u_j'} \tag{2.18}$$

To include all the turbulence the value for k should be included in the TKE. To summarise this means that the total TKE consists of the velocity fluctuations as well as small-scale TKE, see Equation 2.18. However, the contribution of k_{model} is negligible compared to the contribution of the velocity fluctuations. The magnitude of k_{model} is 2 orders of magnitude smaller than the velocity. In the result section is the contribution of k_{model} neglected. For comparison with other literature the velocity and TKE have been non-dimensionalized.

$$u^* = \frac{\overline{u}}{u_0} \tag{2.19}$$

In Equation 2.19 the velocity is dimensionless based on the depth-average free stream velocity, which is 0.214 m/s. The non-dimensionalization isdone for the fluctuations as well, where u^*_{rms} is the non-dimensional version of u^*_{rms}. The non-dimensional TKE is slightly different.

$$TKE^* = \frac{TKE}{u_0^2} \tag{2.20}$$

In Equation 2.20 the TKE is made dimensionless with the depth-average velocity squared. In OpenFOAM the pressure is calculated as the kinematic pressure.

$$p = \overline{p}_{kinematic} * \rho \tag{2.21}$$

In OpenFOAM the kinematic pressure is calculated in the output file p. Using the density of water at 20°$Celsius$ the static pressure is calculated. The pressure in the figures is in Pa, because the pressure has not been compared to other literature in this study.

$$\tau^* = \frac{\overline{\tau}}{\tau_0} \tag{2.22}$$

The bed shear stress is made non-dimensional based on the bed shear stress (τ_0) calculated at the end of the flume for the IC, see Equation 2.22. Further has the fluctuations in bed shear stress been calculated.

$$\tau = \overline{\tau} + \tau' \tag{2.23}$$

In this case the bed shear stress is decomposed using the same method as the Reynolds Averaging, see Equation 2.23. The root-mean-square is calculated for the fluctuations in bed shear stress, which is given by $\tau_{rms} = \sqrt{\overline{\tau'^2}}$

Chapter 3

Results

3.1 Validation

To validate the model and to answer sub-question 1, simulation 2 has been compared to the experimental data of Kitsikoudis et al. (2017). In Figure 3.1a the experimental results are visualized, the results look quite similar to the numerical results in Figure 3.1b. The largest part of the simulation is within a 10% difference with the experimental results. There is a slightly longer wake for the numerical results. However, the largest differences are close to the bottom, as visible in Figure 3.1. The differences are that close to the cylinder the model overestimates the velocity and slightly further around x/D = 2 the model underestimates the velocity. This can be caused by the model or less accurate experimental data near the bottom as these are harder to measure.

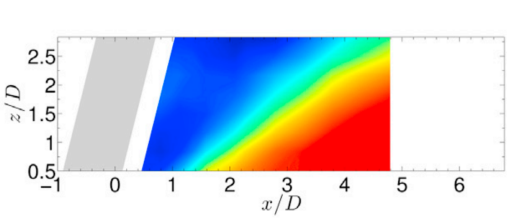

(a) Experimental results Kitsikoudis et al. (2017), with the same colour scale as Figure 3.1b

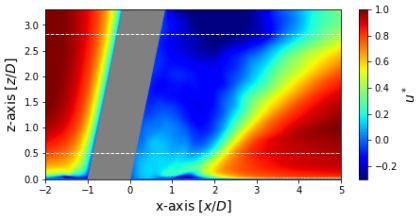

(b) Numerical results of simulation 2: Inclined cylinder with flat bed

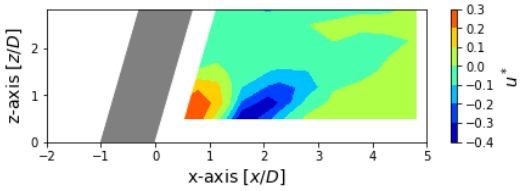

(c) Difference plot reproduced from Kitsikoudis et al. (2017), positive means model predicts higher velocities and vice versa

Figure 3.1: Normalized time-averaged streamwise velocity. In grey the inclined cylinder is depicted. The warm colours represent the velocities in downstream direction and cold colours represents velocities in upstream direction. The white dashed lines indicate the area measured by Kitsikoudis et al. (2017).

The turbulent parts of the numerical simulation and experiments are compared in Figure 3.2. The agreement between the fluctuations in streamwise direction are plotted in Figure 3.2. The pattern of the fluctuations in the model is quite similar to pattern in the experiments. In Figure 3.2 the fluctuations are mostly underestimated, but relative to the depth-average free stream velocity the differences between the model and experiments are very low.

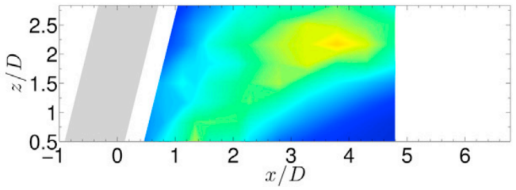

(a) Experimental results from Kitsikoudis et al. (2017), with the same colour scale as in Figure 3.2b

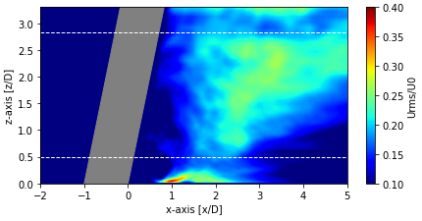

(b) Numerical results

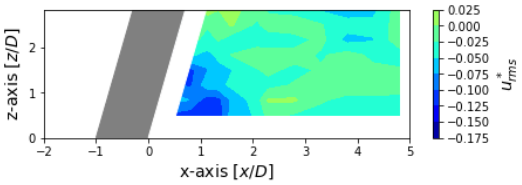

(c) Difference plot reproduced from Kitsikoudis et al. (2017), positive means model predicts higher velocities and vice versa

Figure 3.2: Normalized time-averaged streamwise velocity fluctuations. In grey the inclined cylinder is depicted. The white dashed lines indicate the area measured by Kitsikoudis et al. (2017). Dark blue means there are no velocity fluctuations in a specific direction. Warmer colours indicate a larger fluctuation.

In the horizontal plane at z/h=0.65 the differences are even smaller. z/h=0.65 is Figures 3.1 and 3.2 at x/D = 2.2. Across this plane the differences are smaller in the symmetry line, which can also be seen in Figure 3.3. There can be seen a slight dip in the wake around x/D = 2 in Figure 3.3a, which also results in the largest difference in Figure 3.3e. The trend is that in Figure 3.3e close to the symmetry-axis the mean velocity is underestimated and at the boundary of the wake the velocity is overestimated. For the fluctuation in the streamwise direction this is the other way around, where close to the symmetry-axis the velocities are overestimated and further away there is a general underestimation. The differences are very small between experiments and simulations. Qualitatively, the simulations show the same pattern and thus gives this confidence in the model. Quantitively, the model shows some differences, but is in general close to the measured values. This is also expected, as the RANS-simulations are not solving all turbulent structures (Spalart, 2009).

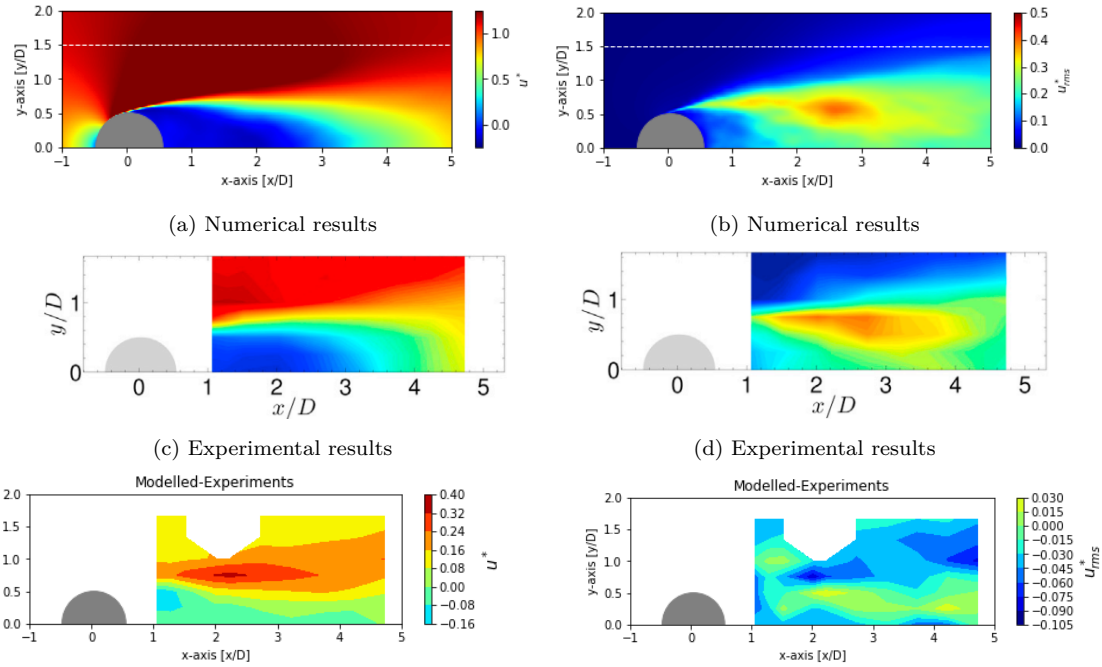

(a) Numerical results

(b) Numerical results

(c) Experimental results

(d) Experimental results

(e) Difference in time-averaged streamwise velocity. Data is reproduced from Kitsikoudis et al. (2017)

(f) Difference in the streamwise fluctuations. Data is reproduced from Kitsikoudis et al. (2017)

Figure 3.3: Experimental and modelling results at z/h = 0.65 for on the left the time-averaged streamwise velocity and on the right the time-averaged streamwise velocity fluctuations u_{rms}. In grey the cylinder is depicted. The white dashed line shows the area measured by Kitsikoudis et al. (2017). The white gap is missing in the data from Kitsikoudis et al. (2017) and therefor is not included in the difference plots

Simulation 2 with an inclined cylinder has been compared to the experiments of Kitsikoudis et al. (2017). Also the results of simulation 1 with a straight cylinder can be compared to the experiments. The comparison for u^* and u^*_{rms} can be seen in Appendix A.

3.2 Simulation 1: Straight cylinder with flat bed

The normalized time-averaged velocities in streamwise direction can be seen in Figure 3.4. The normalized time-averaged transverse velocities have not be included, because the case is symmetric and therefore the time-average flow velocity is expected to be 0. This also leads to small transverse velocities in transverse direction as the maximum and minimum transverse velocities are between $-0.11 < \frac{v}{u_0} < 0.096$. The main part of the symmetry plane varies with a with a range of $0.025u_0$ below or above 0. The largest transverse velocities are seen in the HV downstream of the cylinder.

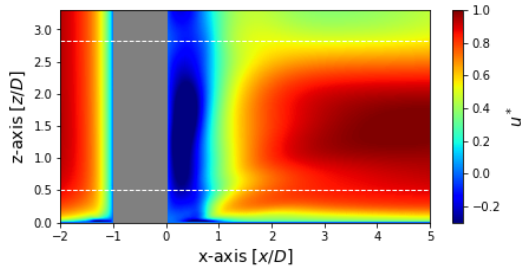

(a) Streamwise velocity, the white dashed lines denote the area measured by Kitsikoudis et al. (2017)

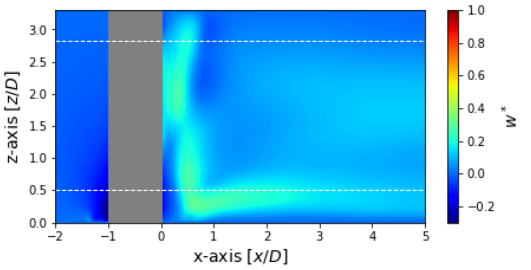

(b) Vertical velocity

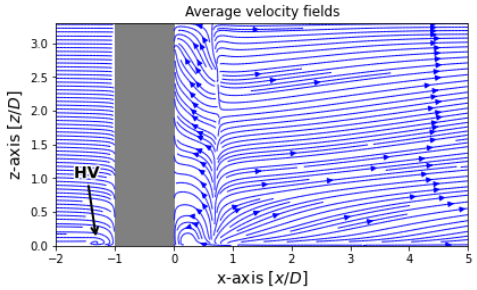

(c) Time-average flow field

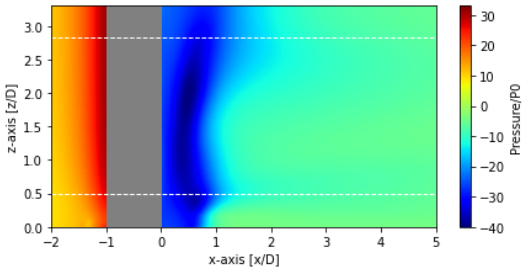

(d) Pressure

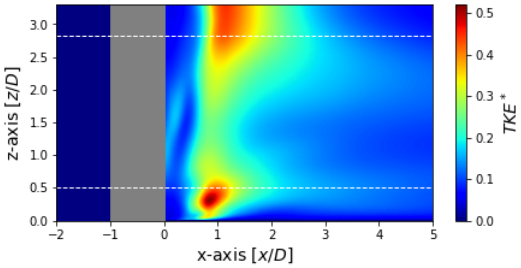

(e) TKE

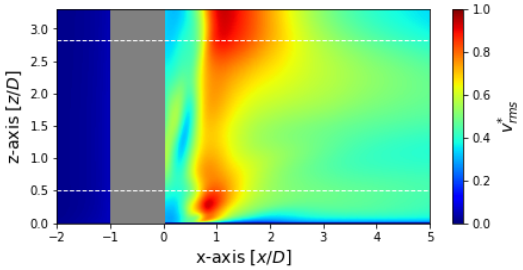

(f) Transverse velocity fluctuations

Figure 3.4: Time-averaged normalized velocity

In Figure 3.4a can be seen that before the cylinder the velocity decreases. In the wake behind the cylinder negative values for the velocity are seen. At the water surface the velocities are lower, which is likely caused by the rigid-lid boundary condition. In the experiments this part of the water was not measured as the water it is hard to measure and very turbulent. The vertical velocities are mainly concentrated downstream of the cylinder in the wake. Combining Figure 3.4a and 3.4b results in Figure 3.4c. In front of the cylinder the streamlines bend towards the bottom of the bed, resulting in the HV, see Figure 3.4c. Downstream of the cylinder a vortex is also visible in the wake in Figure 3.4c. The water passes the cylinder mostly perpendicular resulting in less upflow except in the wake of the cylinder, see Figure 3.4b and 3.5. Another thing that can be noticed is that the HV almost reconnects behind the cylinder in the wake in Figures 3.5. The reconnection of the HV can also be seen in the fluctuations of the velocity at the bottom around $x/D = 1$ in Figures 3.4f and 3.4e. The TKE and largest fluctuation are shown in Figure 3.4e and 3.4f. The transverse velocities are quite large compared to the fluctuations in transverse and vertical direction. This also leads to the fact that the TKE has the same pattern, which is shown in Figure 3.4e. There are small fluctuations inside the recirculation zone, but the largest fluctuations are in the transition

between the recirculation zone and streamwise flowing part of the flow.

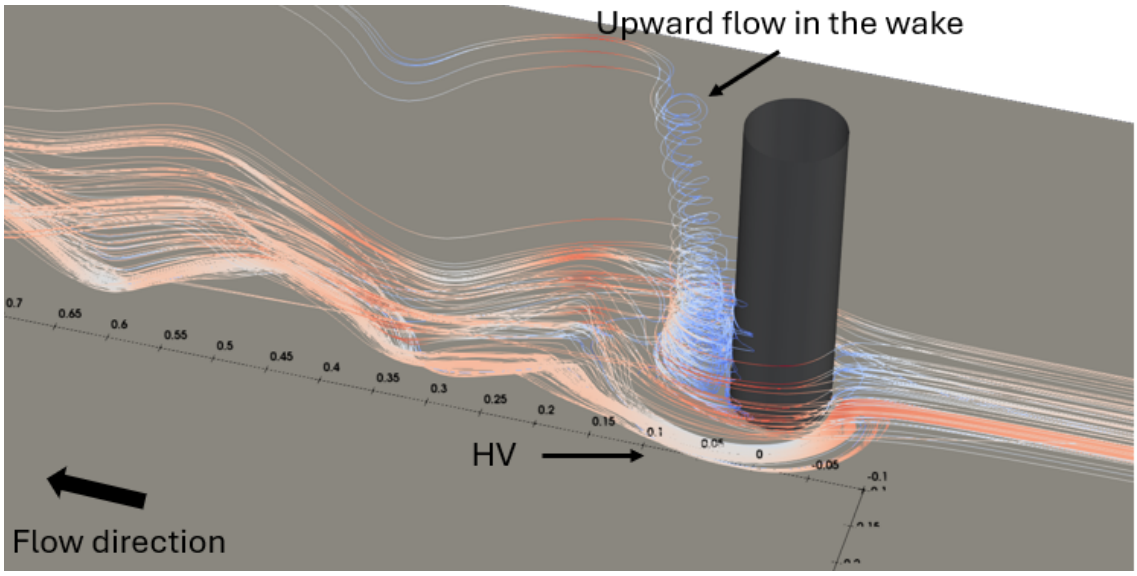

Figure 3.5: Instantanous streamlines (Blue means low velocities and red are high velocities, note that the distances are in meters)

The fluctuations in the velocity are relatively low for the streamwise and vertical direction compared to the transverse direction, which can be seen in Figure 3.4f. The largest fluctuations happen at the water surface and near the bed, where the HV intersects the symmetry plane. The fluctuations in streamwise direction are relatively close to the cylinder compared to the transverse fluctuations, which are further downstream of the cylinder. Also the magnitude of the fluctuations is more than twice as high for the transverse direction.

In Figure 3.6 the vortex shedding is visualized with instantaneous velocity magnitude. From Figure 3.4a can be concluded that in the lee-wake the velocities are mainly upstream directed, as this is not shown in these Figures. In the six Figures half of the shedding period is covered, which is around 2.1 seconds of $f \approx 0.48$, based on the time frames. This leads to a Strouhal number of $st = fD/U_0 \approx 0.2$, which is also corresponding to the Strouhal number found by Kitsikoudis et al. (2017). Behind the cylinder in wake the shedding of the vortices is clearly visible. After the vortex shedding, the vortices are advected with the flow in downstream direction.

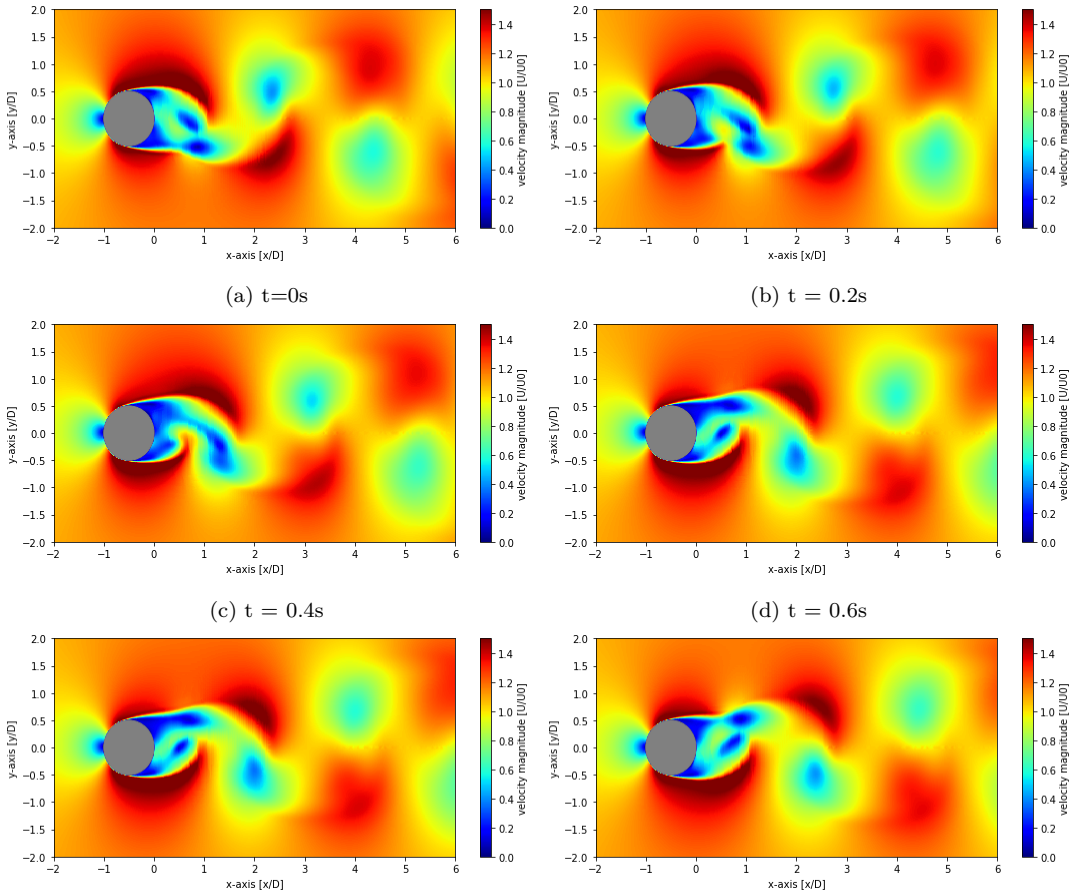

(a) t=0s (b) t = 0.2s

(c) t = 0.4s (d) t = 0.6s

(e) t = 0.8s (f) t = 1s

Figure 3.6: Lee-wake vortices along a half a shedding period at z/h = 0.65 for a straight cylinder depicted in grey. The cold colours represent lower velocity magnitudes and the warm colours represent high velocities.

3.3 Simulation 2: Inclined cylinder with flat bed

In Figure 3.7 the time-averaged streamwise and vertical component of the velocity are shown. Behind the cylinder there is a clear wake visible, which increases over the depth. Especially at the bottom of the simulation the vertical velocities are higher and upward directed. If both plots are combined, this leads to Figure 3.7c. There can be seen that upstream of the cylinder the velocities decrease, and tend to go downward below $z/D \approx 1.2$. Above this point the streamlines bend upward. At the $z/D \approx 1.2$ downstream of the cylinder also a vortex is created. In Figure 3.7d the normalized pressure is visualized. There can be seen that at the upstream part of the cylinder the HV has a lower pressure, as well that the pressure in front of the cylinder increases with the depth. Furthermore can be seen that downstream of the cylinder the pressure is negative in the wake. The maximum pressure is comparable to the pressure in Simulation 1. However, the minimum negative pressure increased from -40 Pa for the straight cylinder to -22 Pa for the inclined case.

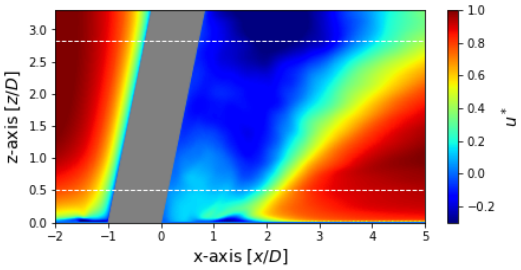

(a) Normalized time-averaged streamwise velocity

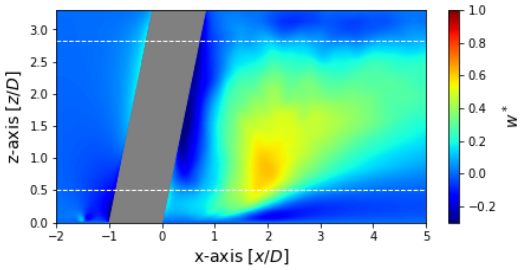

(b) Normalized time-averaged vertical velocity

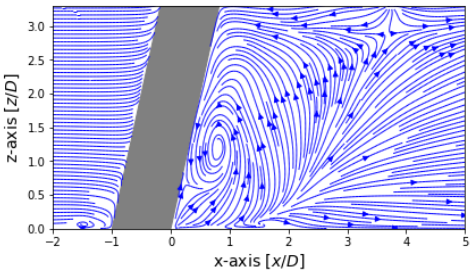

(c) Time-average flow fields

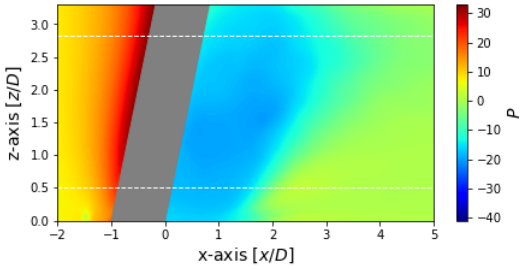

(d) Pressure

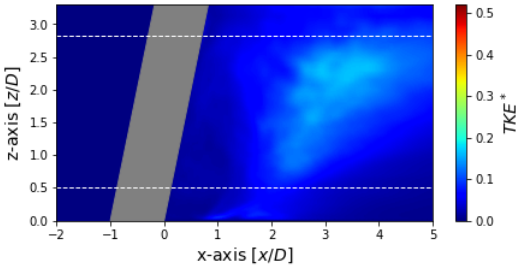

(e) Normalized TKE

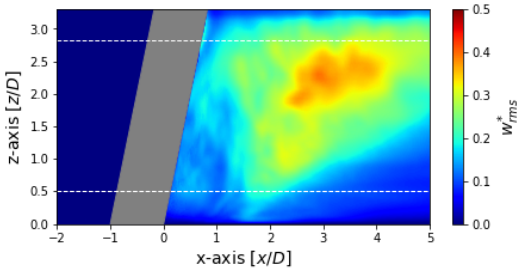

(f) Normalized time-averaged vertical velocity fluctuations

Figure 3.7: Normalized time-averaged velocities, where in grey the cylinder is depicted. The dotted white lines indicate the area measured by Kitsikoudis et al. (2017).

Besides the average velocities in Figure 3.7 also the TKE and the main fluctuation are shown in Figures 3.7e and 3.7f. There can be seen that the main contribution in the turbulent kinetic energy is the vertical fluctuations, where for the straight cylinder the main contribution was from the transverse direction and partly the streamwise direction. The contributions of the transverse en streamwise direction are shown in Appendix C.
Figure 3.7c shows that the flow bends upward upstream of the cylinder, but in Figure 3.8 can be seen that the streamlines cross the cylinder perpendicular. The fact that the pressure is higher in the horizontal plane, than perpendicular to the cylinder might be one of the reasons that the flow crosses the cylinder perpendicular.

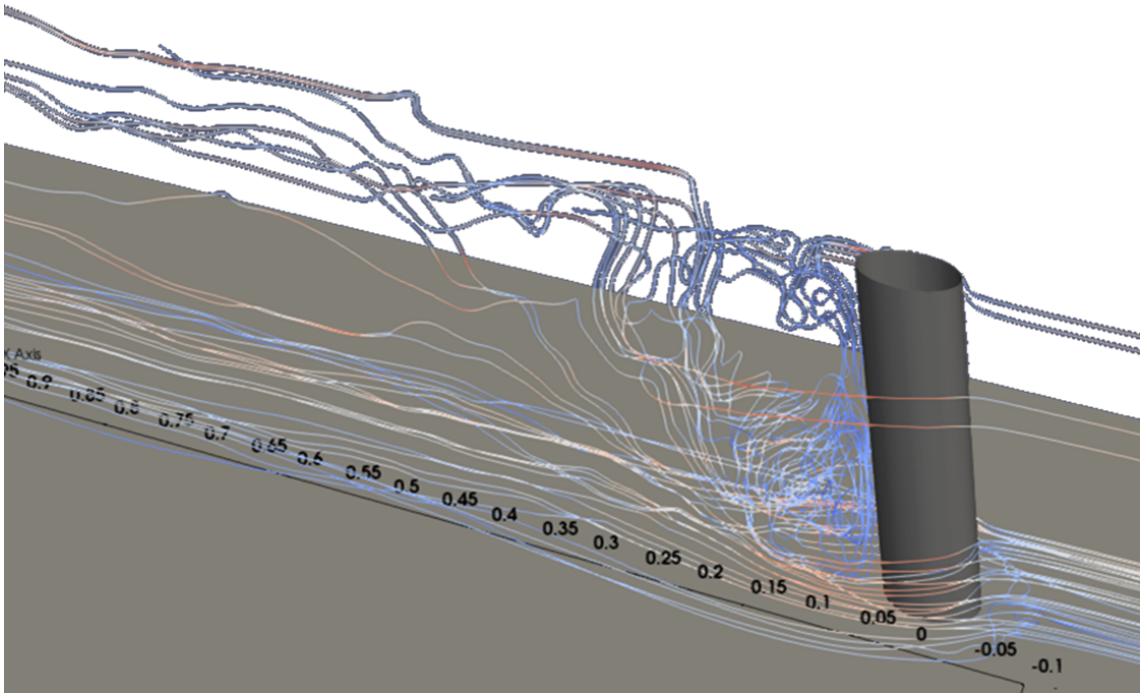

Figure 3.8: Instantaneous streamlines around an inclined cylinder with flat bed (Blue indicates low velocities and red are high velocities, note that the distances are in meters).

In Figure 3.9 the instantaneous results are presented. In contrast to the straight cylinder no clear pattern in the vortex shedding can be recognised. There are no clear lee-wake vortices behind the cylinder as well as there is no clear upflow in the wake. This is likely caused by the pressure gradient which is not as large as for the straight case, but also the increase in vertical velocity and vertical velocity fluctuations. . Around $x/D = 3$ the vortex shedding occurs and vortices leave the wake.

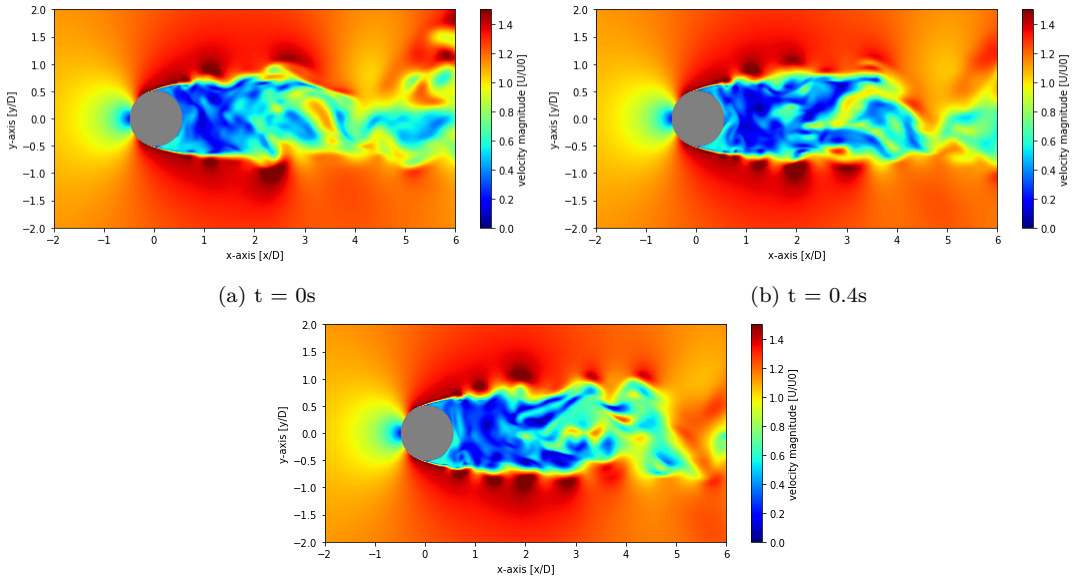

(a) t = 0s

(b) t = 0.4s

(c) t = 0.8s

Figure 3.9: Instantaneous results at z/h = 0.65 for an inclined cylinder depicted in grey. The cold colours represent lower velocity magnitudes and the warm colours represent high velocities.

3.4 Simulation 3: Straight cylinder with scoured bed

In Figure 3.10 the time-averaged velocities can be seen. In Figure 3.10a the wake is clearly visible. Further can be seen that the wake increases over the depth. Upstream of the cylinder at the bottom the streamwise velocities are also very low. These are the location where the HV are. In Figure 3.10b can be seen that close to the cylinder between $-0.3 < z/D < 1$ there is a large flux in upward direction immediately after the cylinder. A combination of these two plots leads to the arrow plot in Figure 3.10c, where the horseshoe vortex can clearly be visualized. Behind the cylinder a circulation zone is created near the water surface, where in the flat bed case a smaller circulation is close to the bottom. Another change is that the width of the wake is not changing over the depth for Simulation 1, but it changes for the scoured bed.

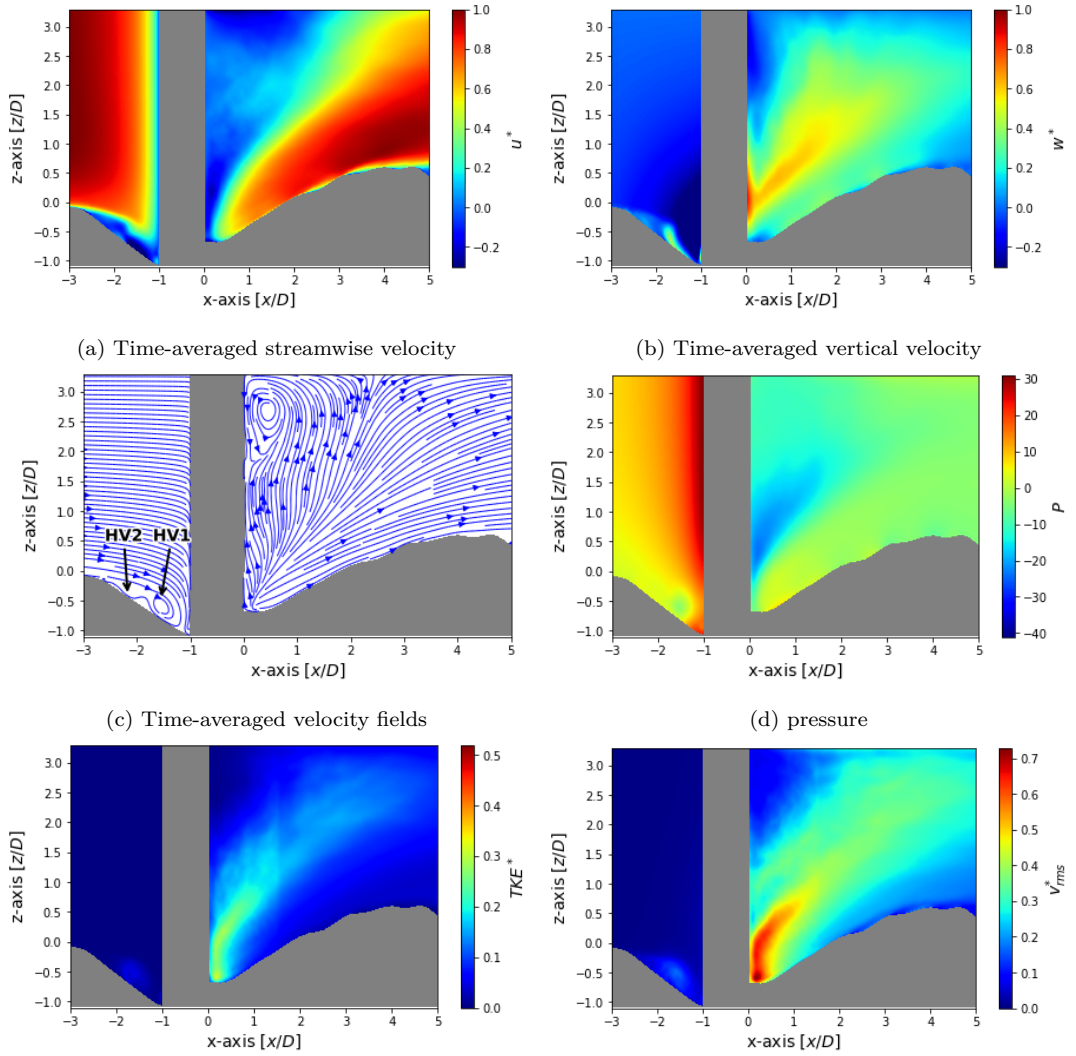

(a) Time-averaged streamwise velocity

(b) Time-averaged vertical velocity

(c) Time-averaged velocity fields

(d) pressure

(e) TKE

(f) Transverse direction

Figure 3.10: Time-averaged velocities for a straight cylinder in a scoured bed. The grey area is the scoured bed and the cylinder.

For the vertical cylinder with a flat bed the largest fluctuations were in transverse direction, this is also the case for the scoured bed, see Figure 3.10f. In this case the highest fluctuations are close to the bottom inside the scour hole. That is slightly different for the vertical fluctuations, which are further from the bed, but still follow the contours of the bed. The fluctuations generally happen now closer to the cylinder and mainly inside the scour hole. There is a low pressure zone, see Figure 3.10d. There the minimum pressure is $-24p_0$, this is already much lower than the minimum pressure from Simulation 1 ($-40p_0$). The decrease in pressure difference corresponds to a smaller pressure gradient at the cylinder. This indicates that the scour hole makes the flow field more streamlined, compared to the flat bed simulation. That the case is more streamlined is also visible in the observation that the TKE decreased, see Figure 3.10e.

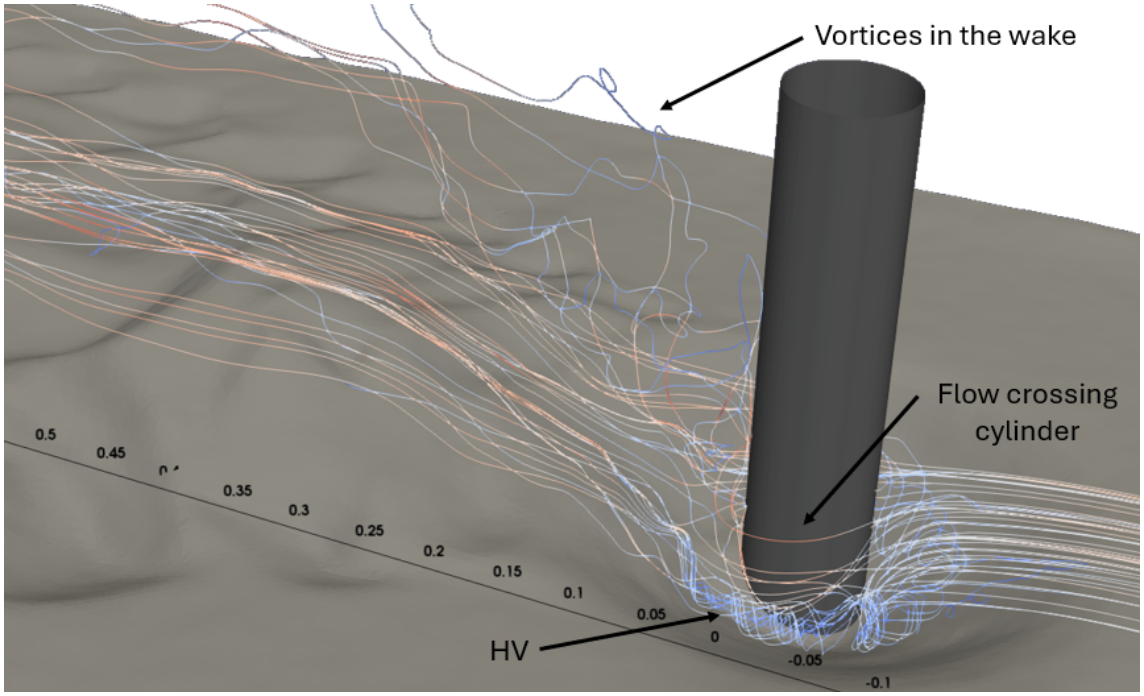

Figure 3.11: Instantaneous streamlines (Blue means low velocities and red are high velocities, note that the distances are in meters)

To understand the dynamics between the bed and the flow field, we can look at the instantaneous streamlines in Figure 3.11. Inside the scour hole the HV can be identified, as well that the wake is also very clear. Most of the flow in the HV follow the bed to leave the scour hole around the symmetry axis. In Figure 3.11 is visible that the flow inside the scour hole crosses the cylinder under an angle instead of perpendicular. Another interesting thing is that the circulation at the water surface in Figure 3.10c is not visual in this plot. There is some circulation, but the streamlines tend to go in streamwise direction. From there we can see that the 3D mixing is important in this case.

3.5 Simulation 4: Inclined cylinder with scoured bed

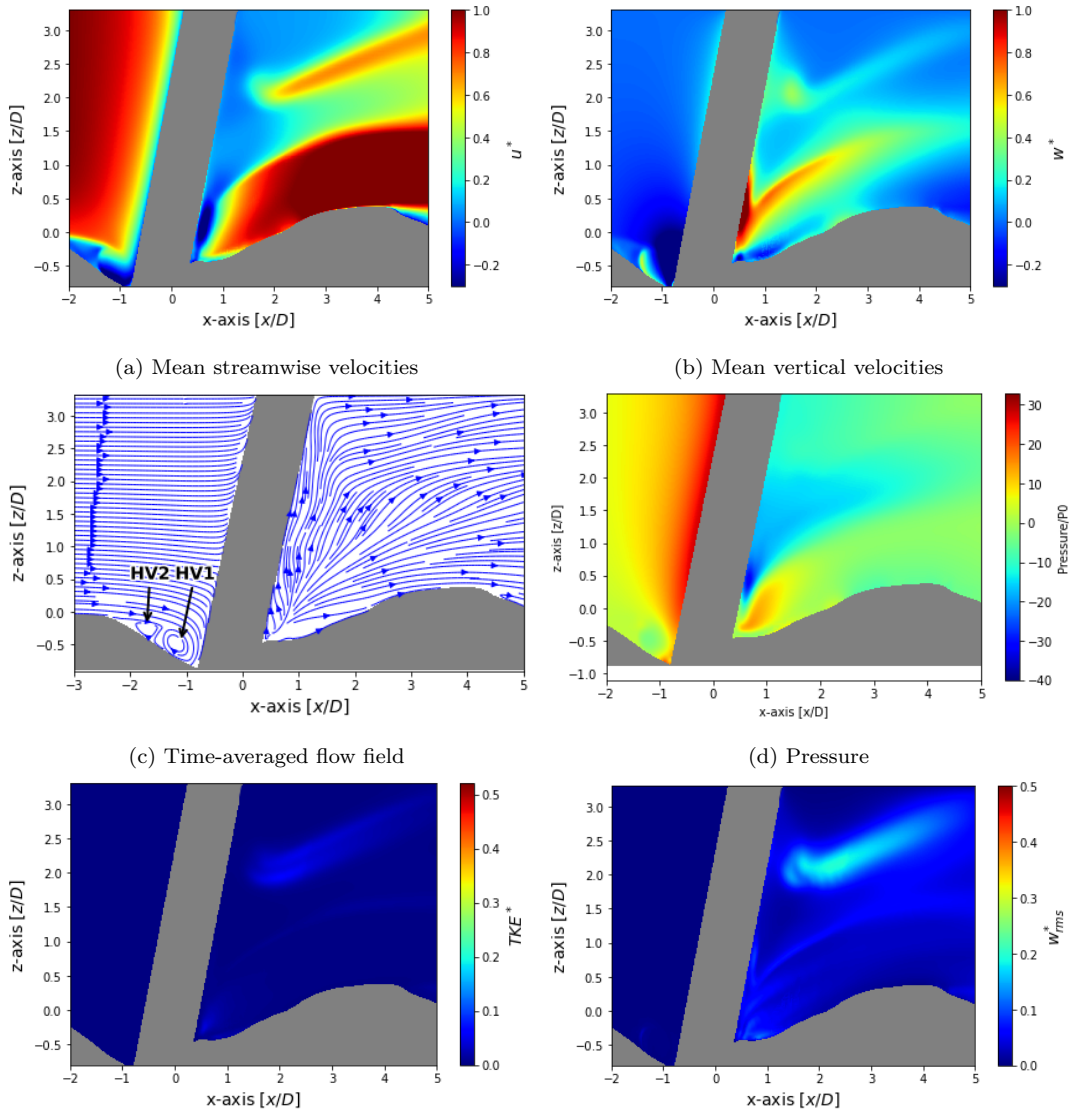

(a) Mean streamwise velocities

(b) Mean vertical velocities

(c) Time-averaged flow field

(d) Pressure

(e) TKE

(f) Normalized vertical velocity fluctuations

Figure 3.12: Results of the scour simulation for 14 degrees of inclination, where in grey the scoured bed and cylinder are depicted

In Figure 3.12a the streamwise average velocity are shown. The velocity before the cylinder decreases, similar to the other cases. Behind the cylinder there is a clear increase in streamwise velocity from the flow leaving the scour hole. At x/D = 1.5 and starting at z/D = 2 is also an increase in velocity. The increase in velocity is likely caused by the flow crossing the cylinder perpendicular, leading to lower velocities near the water surface, but higher velocities around the mentioned area. The flow in upstream of the inclined cylinder with flat bed starts to bend towards the water surface around $z/D = 1.2$, for a scoured bed the bending of the streamlines perpendicular to the cylinder is now around $z/D = 0.75$. The upstream streamlines are now at the start already bended more

downward compared to a flat bed. A distinction between upward moving and downward moving water is around $z/D = 1$, which also is visible in Figure 3.12b. A phenomenon is that there is a large transverse direction of the flow at z/D = 2, which has almost the same slope as the bed and there is a sudden increase in velocity, see Figure 3.12a. In the instantaneous series and the arrow field the existence of the horseshoe vortex system is clearly visible inside the scour hole. Compared to the flat bed simulations there are two HV visible in Figure 3.12c. From Figure 3.12d can be concluded that the maximum negative pressure is higher for the scoured case, but the maximum positive pressure decreases to 29 Pa.

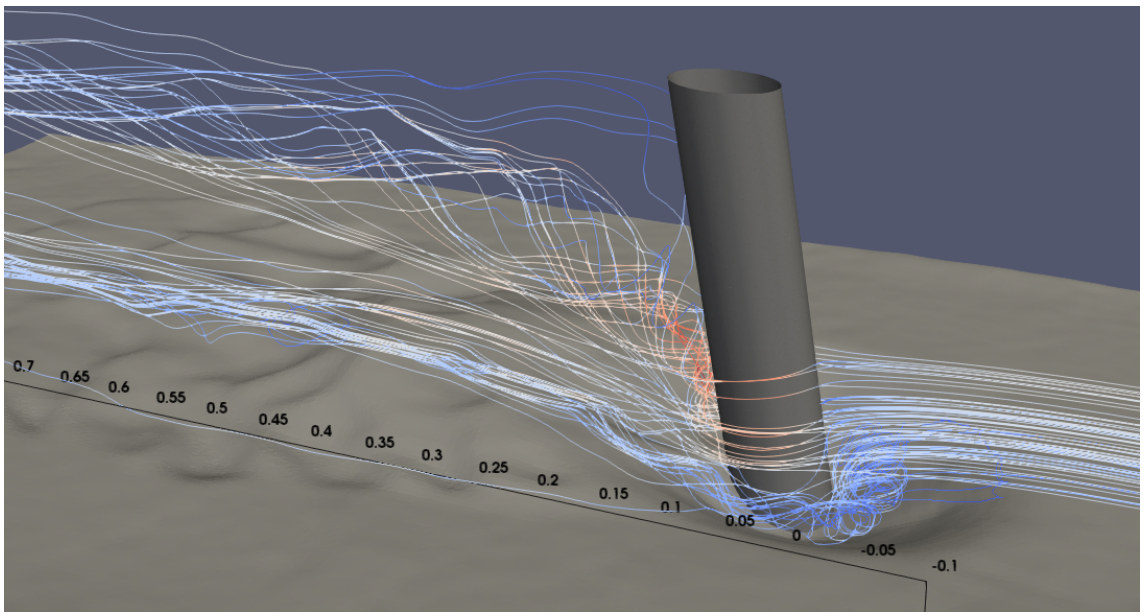

Figure 3.13: Instantaneous streamlines (Blue means low velocities and red are high velocities, note that the distances are in meters)

In the figures above the fluctuations are visible. It is clearly visible that the fluctuations are smaller than for a flat bed. Further is the flow much more structured compared to the flat bed simulations. The largest fluctuations are in the vertical direction, same as for the flat bed, but now the overall turbulent kinetic energy has decreased even more, which reduces the turbulent mixing of the streamlines.

3.6 Bed shear stresses

In Figure 3.14a the contours of the bed shear stress are shown for simulation 1. In simulation 1 the maximum bed shear stress amplification is $7.9\tau^*$. For the inclined case with a flat bed the maximum amplification decreases to $5.1\tau^*$, see Figure 3.14b, where the bed shear stress is also more elongated in streamwise direction. The decrease in bed shear stress is attributed to the decreasing strength of the horse shoe vortex. Due to the fact that part of the flow field upstream of the cylinder is upward directed and thus reducing the strength of the HV, see Figure 3.7c. Compared to Figure 3.14a the bed shear stress is now more elongated into streamwise direction. This can also be seen in Figure 3.8 where the streamlines contract also slightly behind the cylinder and have a high velocity. This

causes to have a locally higher bed shear stress at this point compared to the straight cylinder.

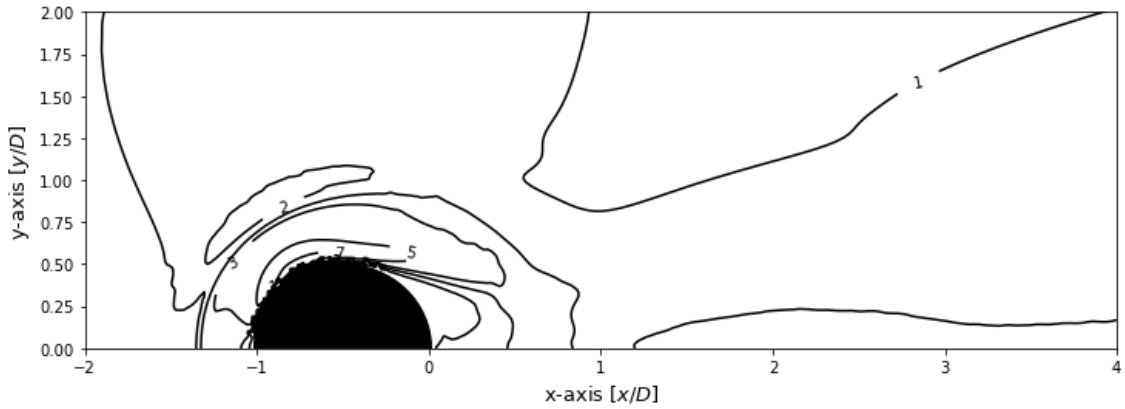

(a) Simulation 1: Flat bed - 0° inclination

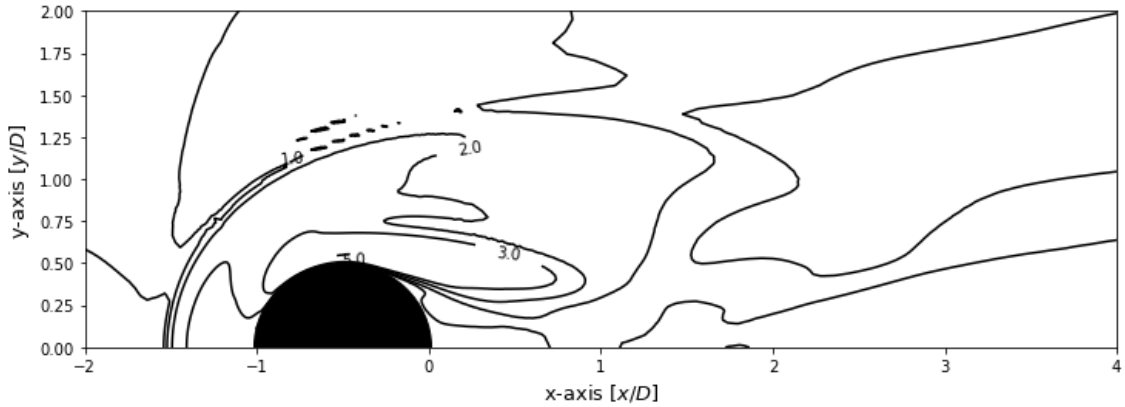

(b) Simulation 2: Flat bed - 14° inclination

Figure 3.14: Contours of normalized bed shear stress (τ^*) for the flat bed simulations

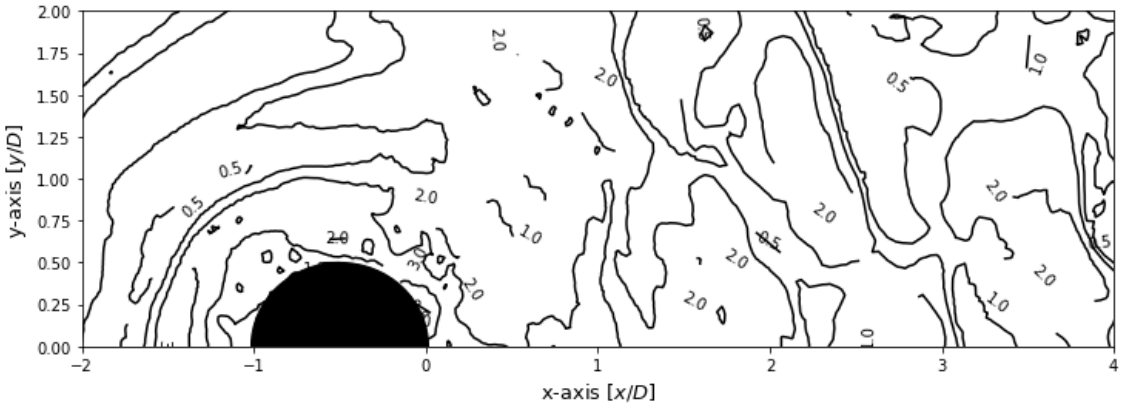

(a) Scoured bed - 0° inclination

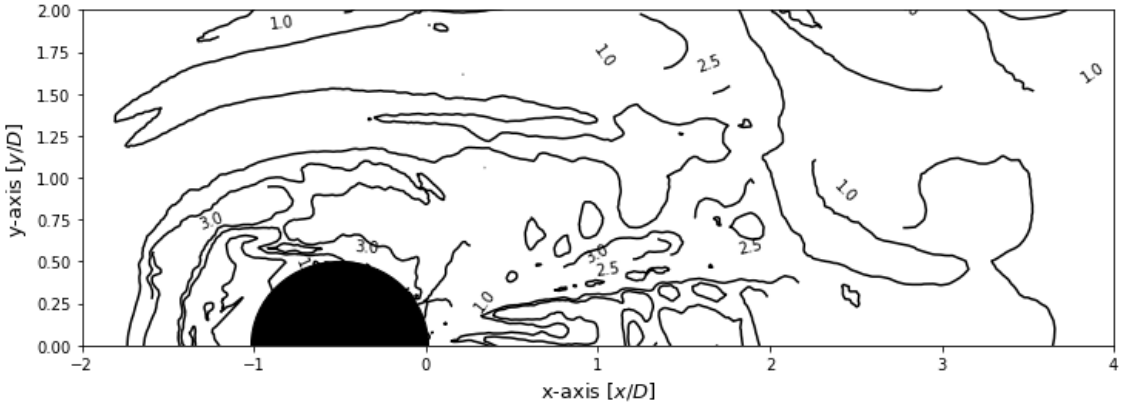

(b) Scoured bed - 14° inclination

Figure 3.15: Contours of the normalized bed shear stress for the scour simulations

The bed shear stress of the scoured bottom has a lower amplification than a flat bed. The maximum amplification decreased from $7.9\tau_0$ to $3.7\tau_0$ compared to the flat bed case. The scoured bed used in the simulation is the equilibrium, which means that no more sediment transport is expected. Because the sediment transport is related to the bed shear stress the bed shear stress should be reduced compared to the flat bed scenario. The location of the maximum bed shear stress is upstream of the cylinder in the HV, the other higher values are at the relative higher points of the sediment ridge behind the scour hole. As now the maximum amplification is in upstream of the cylinder the main contributor to the bed shear stress is the HV, which is also expected as the contraction of the streamlines is decreased, due to the space in the scour hole. In simulation 4 the maximum bed shear stress has increased. The maximum amplification of the bed shear stress is $4.8\tau_0$. Again, the HV is the main source for the bed shear stress amplification. Again downstream of the cylinder relatively high values for bed shear stress are found, which are at the higher elevated parts of the sediment deposition. But compared to simulation 3, also high values ($\overline{\tau} > 3\tau_0$ are observed.

The bed shear stress has also some variation over time. These fluctuations can also initiate sediment transport (Zanke, 2003). The time-average bed shear stress might not be sufficiently high to initiate the sediment transport, but with the fluctuations the sediment transport initiation can take place. These root-mean-square fluctuations are plotted in Figure 3.16a. The fluctuations are

relatively smaller than the maximum amplification of the bed shear stress. A normalized fluctuation of $1.37\tau^*_{rms}$ is calculated for simulation 1. The largest variation are downstream of the cylinder, especially in the zone where the HV reconnects, which is again similar with the large fluctuations in the velocity at x/D=0.5 in Figure 3.4e. Due to the connection of the HV large velocity fluctuations are present near the bottom. These fluctuations in velocity means that there are different velocity gradients, resulting in different values for the bed shear stress.

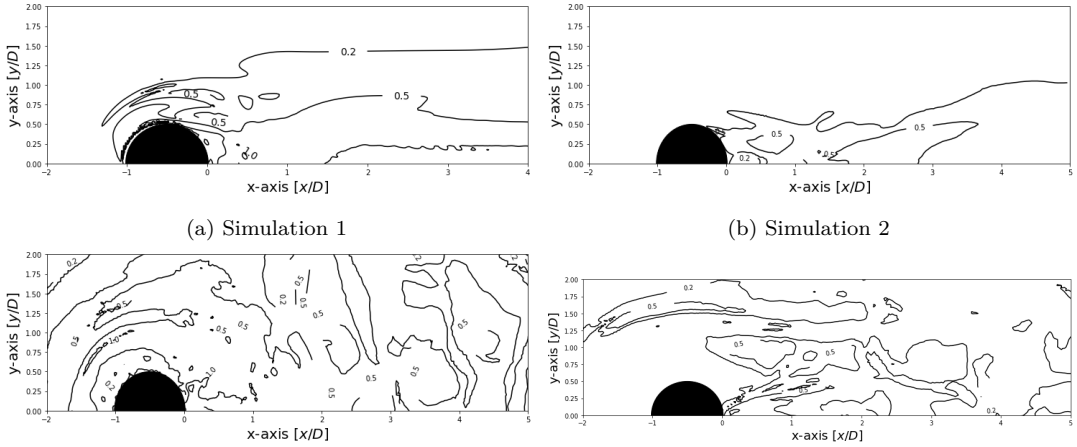

(a) Simulation 1

(b) Simulation 2

(c) Simulation 3

(d) Simulation 4

Figure 3.16: Fluctuations in the bed shear stress in τ^*_{rms}

Where for the straight cylinder there were small deviations in the bed shear stress at the reconnection of the HV, most of the fluctuations happen in the wake further behind the cylinder as there are also large deviations over time in the velocity and thus in the velocity gradient, due to the shedding of vortices. In case of simulation 3 and 4 the bed shear stress fluctuations are more spread over the bottom and also more present upstream of the cylinder at the cross-over between the scour hole and the undisturbed bed. The maximum fluctuation has decreased for the scoured cases to around $\tau_{rms}/\tau_0 \approx 1$.

Chapter 4

Discussion

In the previous Chapter the results are shown for the different cases. In this chapter the results will be discussed. First the results will be compared to the literature. And the second part consists of a discussion based on the numerical simulation and methodology used in this research.

4.1 Comparison to literature

4.1.1 Simulation 1: Straight cylinder with flat bed

The first simulation is with a flat bed and a straight cylinder. The flow structure is slightly different compared to the simulation from (Aksel et al., 2021), as they model a free-surface elevation instead of a rigid-lid as in these simulation. Physically, however, the simulation is the same, as the same flume that has been used as for the experimental set-up of Kitsikoudis et al. (2017) and thus also for the simulations. The free-surface elevation leads to a more upward directed flow at the water surface in upstream of the cylinder (Aksel et al., 2021). In the results was a large upflow visible in the wake behind the cylinder, see Figure 3.4c and 3.5. This upward flow is not present in the results of Aksel et al. (2021), where the flow in the wake moves more in streamwise direction. Other studies with a rigid-lid assumption observed the same phenomenon that there was a large upflow present (Aksel, 2023; Baykal et al., 2015). While in free-surface simulations and experiments these upward directed velocities are not present (Aksel et al., 2021; Kitsikoudis et al., 2017).

The bed shear stress is in the same order of magnitude as numerical results of Roulund et al. (2005), which was validated on experimental data. The comparison is shown in Figures 4.1a and 4.1b. The maximum amplification of the bed shear stress is shown in Figure 4.1. However, the location is slightly different. As in the experiments the bed shear stress is more concentrated in front of the cylinder. In this case the bed shear stress is also more focused on the sides of the cylinder, most likely caused by the contraction of the streamlines. This is also the case in the simulations of Y. Liu et al. (2024) and Wang et al. (2020), see Figures 4.2a and 4.2b.

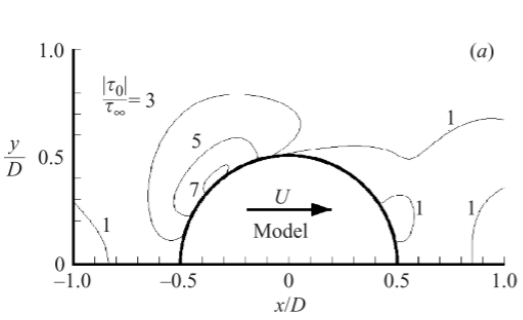

(a) Bed shear stress for straight cylinder with flat bed from Roulund et al. (2005)

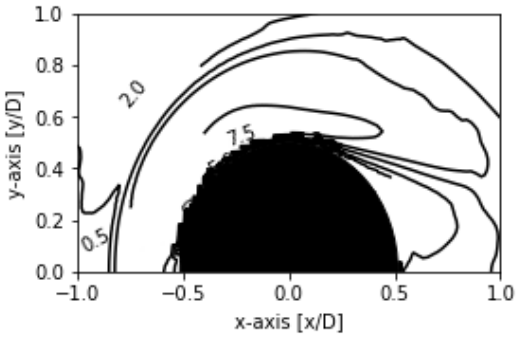

(b) Simulation 1

Figure 4.1: Comparison bed shear stress (τ^*) for simulation 1. The cylinder is represented by the black circle. The contour lines have the magnitude of [0.5,2,3,5 and 7]τ^*

4.1.2 Simulation 2: Inclined cylinder with flat bed

The results of simulation 2 can also be compared to other studies. In the numerical study of Wang et al. (2020) the cylinder is completely under water, which leads to a different flow structure. Where for an emergent cylinder the inclination results in an increase in upflow, this is not the case for a sub-merged cylinder. Downstream of a sub-merged cylinder the down flow increases resulting in a different flow field. Upstream of the cylinder the same pattern is visible that at a certain distance from the bed the streamlines bend upwards to the top of the cylinder (Wang et al., 2020). Far from the bed the influence of the bed is reduced and the results can be compared to the numerical results of Zhao et al. (2009). Their paper focused on an infinite cylinder that is inclined. In their results the flow also follows the cylinder, which is most visible in the results of simulation 4. In their study a more clear structure of vortex shedding is present than in the current simulations. An important factor here is the low Reynolds number of 1000 which is used for this, although the Reynolds number both are in the fully turbulent regime (Zhao et al., 2009). However, Zhao et al. (2009) also notes that the streamwise vortices change from regular to irregular. The irregular vortex shedding can also be seen in the instantaneous velocity in Figure 3.9, where no clear distinction of the vortex shedding is visible.

Due to the weakening of the HV the bed shear stress decreases. A decrease can also be seen in the numerical results of Y. Liu et al. (2024), see Figure 4.2. The results show a similar regions of bed shear stress amplification. Although the amplification in simulation 2 has decreased even more compared to results of Y. Liu et al. (2024).

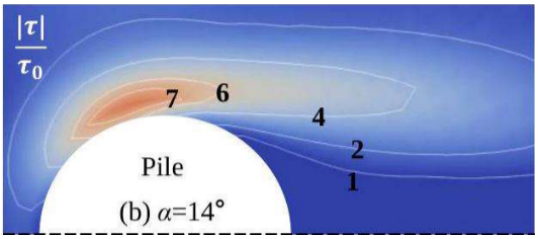

(a) Bed shear stress for an inclined cylinder with flat bed from Y. Liu et al. (2024)

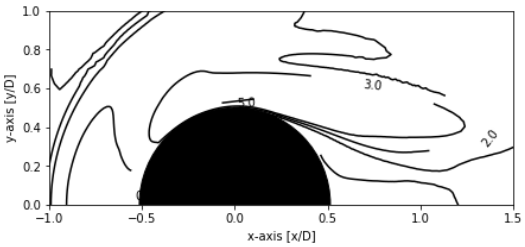

(b) Bed shear stress simulation 2

Figure 4.2: Comparison

4.1.3 Simulation 3: Straight cylinder with scoured bed

The scour hole for a straight cylinder has also been analysed in other literature, a comparison can be made based on these experiments and simulations. In front of the cylinder, the TKE is also the largest near the bottom, where also the HV is. This trend is also visible in the experimental results of (Graf & Istiarto, 2002). In case of the RANS-simulations the larger vortices can be clearly seen in Figures 3.10c and 3.12c. In particular in Figure 3.12c can be seen that the smaller Bottom Attached Vortices (BAV) and a Junction Vortex (JV) are not visible in the simulation, but HV1 and HV2 are present (Kirkil et al., 2008). For the straight cylinder with scour hole some backflow can be observed, but no clear secondary vortex. The flow field is slightly different compared to the numerical results of Aksel et al. (2021), where in the the presented simulations the largest vertical velocities were measured just above $z/D = 0$. In the results of Aksel et al. (2021) the vertical upflow also happens very close to the cylinder, but higher in the water column. The reason could be the difference in the modelling of the free water surface, but also the depth of the scour hole in relation to the water depth might be important.
Another thing that stood out, were the larger transverse velocities for the simulations with scour. Transverse velocities were present in the time-averaged velocities for simulation 3 and 4. To see the structure of these velocities at $x/D = 1$ and $y/D = 1.5$ cross sectional plots are made. These can be seen in Figure 4.3. For the straight cylinder, the transverse velocities are comparable to each other, where the secondary flows are visible at the bottom. For both cases the flow structure is quite comparable and shows the same trends. As in Kirkil et al. (2008) the Detached Shear Layers (DSL) are close together and move upward along x. In simulation 3 a large part of the TKE a result of the vertical velocity, which is causing the increase in a circle, the streamwise fluctuation are causing these legs.

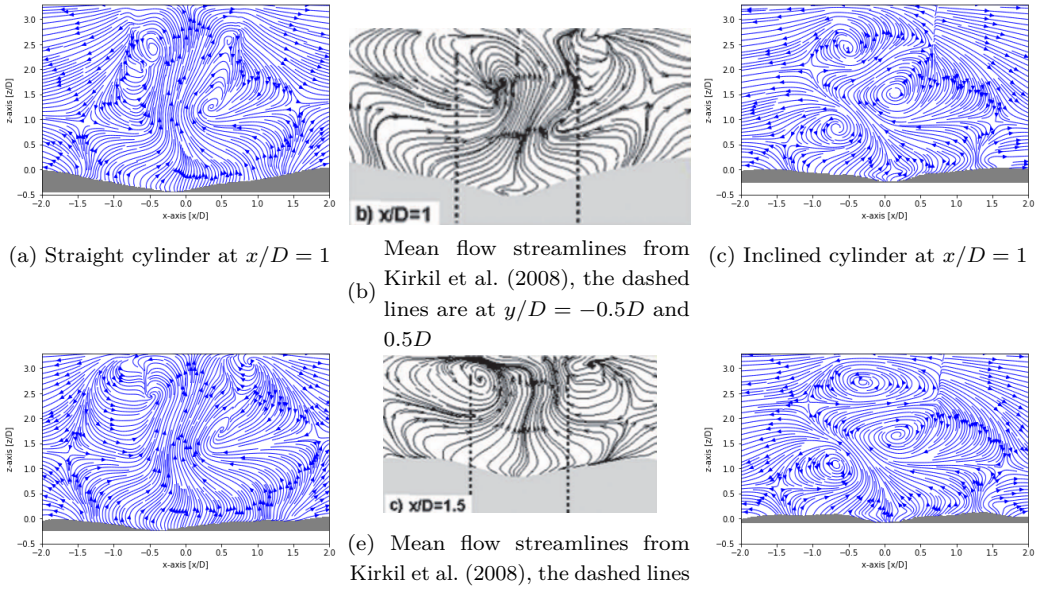

(a) Straight cylinder at $x/D = 1$

(b) Mean flow streamlines from Kirkil et al. (2008), the dashed lines are at $y/D = -0.5D$ and $0.5D$

(c) Inclined cylinder at $x/D = 1$

(d) Straight cylinder at $x/D = 1.5$

(e) Mean flow streamlines from Kirkil et al. (2008), the dashed lines are at $y/D = -0.5D$ and $0.5D$

(f) Inclined cylinder at $x/D = 1.5$

Figure 4.3: Time-average streamlines at different x/D

The difference between the simulations is clearly visible if we compare Figures 4.3c and 4.3a with each other and Figures 4.3d and 4.3f. We can see that in both cases the counter rotating pier-attached vortices play a role, as these are the three large vortices in these Figures. Where in simulation 3 the vortices are further away from the symmetry axis. In the inclined case the vortices in the middle and top are close to the centre line and more above of each other, which results in these high transverse velocities at the symmetry plane. This also results in very locally high velocities in vertical direction. Aksel et al. (2021) used a RANS simulation and also investigated these Large-Scale Counter-Rotating Vortices (LSCRV) and only had 2 LCSRV, where one was more located in the centerline. Compared to the the present results and results of Kirkil et al. (2008) their LSCRV are much closer to the water surface close to the cylinder. The large transverse velocities also have an effect on the TKE in Figure 4.4. The effect of the apostrophe-shaped area from simulation 4 is clearly visible in Figure 4.4.

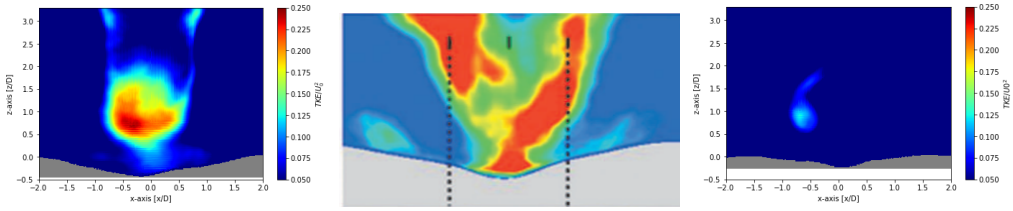

(a) TKE for simulation 3

(b) resolved TKE from Kirkil et al. (2008)

(c) TKE for simulation 4

Figure 4.4: TKE comparison between simulation and an LES-simulation from Kirkil et al. (2008)

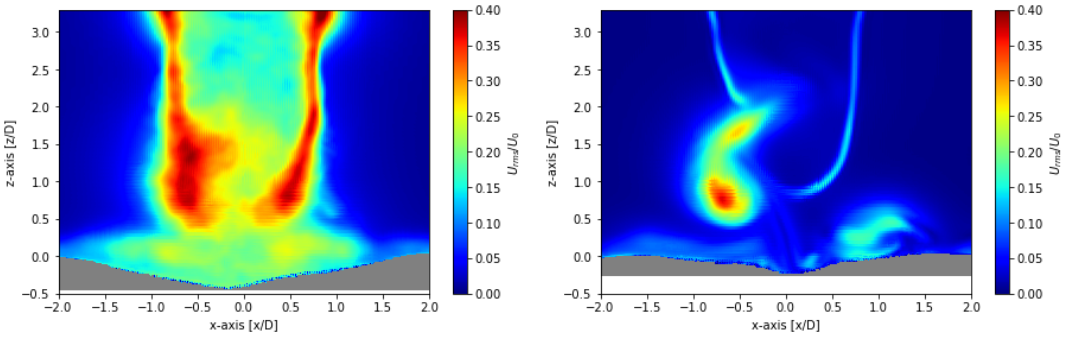

(a) Simulation 3

(b) Simulation 4

Figure 4.5: Time-averaged streamwise velocity fluctuations at $x/D = 1$

The apostrophe-shaped area from Figure 4.4c is visible for the root-mean-square of the velocities in all directions, for the streamwise direction a slight contour of the u-shaped streamwise fluctuations are visible, like in Figure 4.4a. In comparison to the results for an flat bed the fluctuations in streamwise direction decrease and the vertical component becomes even more dominant. Where the results of (Kirkil et al., 2008) suggest that still the streamwise fluctuations are dominant, as Figure 4.5a show the same pattern as the the TKE in Figure 4.3b. The large TKE can also be seen in the results of Graf and Istiarto (2002) where at the largest TKE was measured at $x/D = 1$ around $z/D = 1$. There can be seen that the TKE behind the cylinder is close to the bed at first, but moves towards the water surface for later simulations (Graf & Istiarto, 2002), which is also the case for simulation 3.
To conclude, the straight cylinder shows comparable characteristics in flow field as other simulations, especially in the HV, upflow behind the cylinder (e.g. (Aksel et al., 2021; Baykal et al., 2015) and bed shear stress ((Y. Liu et al., 2024)). This is also the case for the inclined cylinder with the results of Y. Liu et al. (2024) which used the same inclination and flume experiments. Their bed shear stress has the same contours as the results of simulation 2. With the implementation of the scour hole the results could be compared to the same flume used in the simulation of Aksel et al. (2021), where the bed shear stress also decreased as in general was visible. Furthermore were in the RANS-simulation the HV clearly visible. Simulation 4 shows some different results than is expected based on literature as well as the comparison between simulation 1 and 2. We can learn that the large turbulent structures are well modelled in general and these have the largest effect on the flow structure and bed shear stress.

4.2 Model uncertainties

4.2.1 Boundary conditions

One of the uncertainties in a model are the applied boundary conditions. In the first 2 simulations different BCs have been applied for omega, as for simulation 2 a relatively low number for omega has been used. This means that the dissipation at the wall is relatively low for these cases. For the other cases with an omega fixed at the walls of 10 no vortex shedding occurred. There was a wake behind the cylinder, but the velocities inside the wake were also downstream oriented and reached even to the end of the domain. So there was no diffusion present in the simulation. To get the vortex

shedding values for omega in the range from 100-12800 were used. But only after a value of 10000 the vortex shedding occurred again. For values of 100 and 1000 the simulation for IC would also not converge to a solution. This increase in ω is also in the range that is expected based on Equation 2.11. However, if these BC were applied the flat bed there is again a transverse velocity which would not be present in such a scenario. Therefore, it is likely that there is a cause in the BC that leads to a shear force in the model itself. Apart from the fact that these time-averaged transverse velocities should not occur in the water column far from the bed for a flat bed. At a scoured bed the transverse velocities are expected for the simulations as the water flows to the lowest point caused by the pressure gradient, see also in the section above the comparison with the results of Kirkil et al. (2008). To verify the effect of the application of an omega of 10000 also the same value has been used in combination with wallFunctions. However, the simulation with wallFunction yielded the same results. The implementation of a wallfunction yields that different values of omega are used at the wall. For a wallfunction with a fixed value the omega at 10000, the wall fluctuates between 1000 and 10000. In the last simulation, this proved not to influence the results. The wallfunction also has another benefit, as it also makes sure that there is a smooth transition between the viscous and buffer layers, so the different cells along the distance from the bed. A rough transition over the distance to the walls could have been caused by collapsed layer, as not everywhere the bottom was covered by 5 layers parallel to the bottom. Another change in BC has been to verify the effect of the "calculated BC" in Table 2.2. These have been changed to the zeroGradient boundary conditions in OpenFoam at the outlet. However, the change in BC yielded the same results.

In Section 4.1 is already mentioned that the effect for the rigid-lid assumption is likely causing the upward flow in the wake behind the cylinder. Furthermore is the rigid-lid assumption calculated for the straight cylinder case, but in the inclined case can be seen that the flow upstream of the cylinder tends to move up along the cylinder, meaning that the free surface elevation is higher for the inclined cases and has a larger effect on the flow structure near the water surface.

4.2.2 Initial conditions

In Section 2.2.4 can be seen that there is a difference between the simulations with a fixed value of 10 and 10000. This means that there is an effect on the BC and the viscous sub-layer by the energy dissipation. The first impression was that the bed shear stress was linear for the first layers in simulation 2, as the y^+ is above 5. This was also visible at the velocities, which were linear for the first two cells. However, it might that the the boundary layer was not fully developed. This can likely be caused by the relative low dissipation of energy meaning that the flow takes longer to fully develop. Another option to get fully developed flow is to use cyclical boundary conditions. This approach is not possible with the implementation of the added layers feature in snappyHexMesh. Another remark that flow might not be fully developed is the fluctuation in ν_t in Figure 2.4a. In the results was visible that the eddy viscosity is very sensitive for the transition between blocks for both snappyHexMesh and blockMesh. Therefore the fluctuation likely indicates a not fully developed flow or else the mesh transition is not fine enough. Given how close the numerical values were to the experiments the effect of the not fully developed flow is minimal. During the experiments a certain roughness has been applied by the walls, this can partly be modelled by the value for omega in the simulation. This also has clearly an effect on the velocity profile, even when the undisturbed depth-averaged velocity is the same. To validate the velocity profiles, the velocity profile should be

compared to the velocity profile in front of the cylinder in the experiments.

4.2.3 Numerical schemes

Large part of the uncertainties lie inside the model itself. RANS-simulations model part of the turbulence and therefore there will always be a difference compared to the physical truth (Spalart, 2009). Due to the efficiency in simulation time, the RANS-simulation is still a preferred option for a lot of CFD problems. In this research the focus was mainly on the physical processes that play a role. Beside the simplification of modelling part of the turbulence, numerical modelling has more draw backs. In the numerical simulations Backward Euler has been used as the time scheme. As the simulation that is in a transient state an implicit scheme dampens the fluctuation over time(Wilcox, 2010). Therefore is also expected, as also visible in Section 3.1 that the fluctuations are in general underestimated. The benefit of an implicit time scheme is that the model is more stable and a larger timestep can be used compared to an explicit scheme. Furthermore, in the early stages of the research a Detached Eddy Simulation (DES) simulation has been performed. The results of the simulation were completely different than the results of the experiments from (Kitsikoudis et al., 2017). The wake was much larger (until x/D=2) than both the RANS and experiments showed. For the application of flow around a cylinder DES have shown to deliver better results than RANS-simulations (Chang & Constantinescu, 2023). One of the reasons could be the IC for which the velocity profile shows a sharp gradient, see Figure 2.4. As first-order accurate schemes have been used, it could have been an unstable solution, resulting in these relatively high velocities.

4.2.4 The influence of the mesh

In this research there has not be done a sensitivity analysis on the number of cells or mesh independence. The cell size could be too coarse to model turbulence. However, based on other literature the number of cells should be sufficient to model flow around a cylinder. However, if the model would be grid dependent this introduces a small error. Due to the mechanics of snappyHexMesh already a small error is introduced due to numerical diffusion. That makes it most likely also the reason why the DES simulation could only be ran for the BlockMesh model. For the snappyHexMesh simulation the DES-model crashed within seconds. RANS is more robust compared to DES. Therefore it handle these grid changes better (Guerrero, 2021). For the RANS-simulation these schemes are less relevant, as already an error is introduced in the RANS method. Another limitation is that blockMesh allows nice grading for a straight bottoms or nicely curved area‘s like the cylinder. These are important to have a smooth pressure distribution and thus a good model. However, for the implementation of the scour hole a lot of different orientations of the surface normals are present, which make it harder to have the cells parallel to the surface. In Figure 2.9 there can be seen that the small layers near the bottom are added, but close to the cylinder these layers collapsed. More layers lead only to faster collapsing of layers and thus a worse coverage of the bottom. For the flat bed simulations the layers would connect to the cylinder, which is not the case for the scoured bed simulations. There has also been tried to use the blockMesh model in the snappyHexMesh model to intersect with the scoured bed, but due to the grading of the blockMesh model the layers parallel would collapse much faster than for the snappyHexMesh model.
Another point of discussion regarding the mesh is for the mesh of simulation 3 and 4. The bed was curved at the most upstream points of the measured. This part has been extended with 5 cm to make sure that the inlet is flat to get rid of transverse velocities. The extension of the bed also

leads to some errors compared to the physical processes that have played, but the fluctuations are very small in comparison to the effect of the cylinder as well as the ripples in front of the cylinder. Another point is that for simulation 3 the centre of the cylinder was exactly at (x=0,y=0), but this was not the case for simulation 4. As the bottom is also inclined, the exact location of the cylinder is hard to determine. Therefore a small error in the location of the cylinder might be present. This might have had an effect on the pressure close at the bottom in simulation 4, which is much higher compared to the other simulations. Another simulation with a slightly moved cylinder resulted in a worse grid, where at the water surface the added layers would collapse and other unrealistic fluctuations were present. Therefore the most likely explanation for simulation 4 is that the location of the cylinder has resulted in a high pressure zone downstream of the cylinder. Which resulted in the unrealistic velocities.

4.3 Impact on the vegetated foreshore

Generally are in salt marshes lower flow velocities present than u_0 of 0.214 m/s. Further is a diameter of 9 cm used, which would be a tree given the size of the stem. Furthermore, the Reynolds number is high for most flow around vegetation in a salt marsh (e.g. Etminan et al., 2017, 2018). Further is the scour hole very dependent on the grain size and is the influence of the scour depth a factor in the alteration of the flow field. Given the limitations, the focus lies on the qualitative contribution of the bent vegetation.

The modelling of vegetation is important for as the vegetation contributes to the flood safety. The functions of a vegetated foreshore or salt marsh is to stabilize the coastline and to reduce the flood risk. To understand how a salt marsh stabilizes the coast line, it is important to understand how vegetation affects the sediment transport within a salt marsh. The sediment transport around vegetation caused by the vegetation itself is important, since that will determine if the salt marsh will expand or erode. In this study, there can be concluded that the bending of vegetation has a beneficial effect on reducing the sediment transport capacity. The sediment transport capacity is related to the bed shear stress, which is reduced due to the bending of vegetation. The bed shear stress increases even more for dense vegetation (Baptist et al., 2005). In this case the bent vegetation can form a more protective layer around the bottom as the bed shear stress is reduced. In this study, sediment transport has not been included. However, the flow field alteration might have an affect on suspended sediment already present in the. The vertical velocity has increased for bent vegetation and could therefore have an influence on the sediment particles that are present in the water column. In that case other factors would also play a more important role as in submerged vegetation the flow field as in Wang et al. (2020). There the flow field is different compared to the flow field in emergent vegetation, like in this study. In case of reducing the flood risk the bent vegetation has a negative effect. The bending reduces the height relative to the bottom of the vegetation, meaning that the effective height for the vegetation has decreased if applied to the Baptiste Equation (Baptist et al., 2007). Further reduces the bending of vegetation the wave attenuation characteristics of the vegetation (Temmerman et al., 2023). This means that the bending of vegetation is beneficial for stabilizing the coastline, but the effects on flood risk are not ideal as the wave attenuation and friction decreases. Therefore I would suggest to take the effect of bending mainly into account for the flood safety and not as much for the stabilizing of the coastline. To implement the effect on the

sediment transport capacity within a salt marsh a more quantitive study has to be performed.

Chapter 5

Conclusions and Recommendations

The aim of the study is to understand the effect of the inclination of and scour around vegetation on the flow field and bed shear stress. The vegetation is simplified as a cylinder and is therefore also applicable to similar cases in hydraulic structures. In this section the first research question focuses on the validation of the model. In the section section the second and third research question are answered, which focuses on the effect of the inclination of the cylinder on a flat bed. The third section answers the last two research question, where also an equilibrium scoured bed is introduced. The fourth section answers the main research question, where all 5 sub-research questions play a role. The conclusion ends with a recommendation for future research.

5.1 Quality of a RANS-simulation

In order to answer the first research question the results in Section 3.1 are used. In this section the results of simulation 2 (inclined cylinder with a flat bed) have been compared to the experimental results of (Kitsikoudis et al., 2017). The first research question is:

"How does a RANS-simulation that predicts the fluid dynamics around an inclined circular cylinder compare to experimental results?"

Overall are the time-average velocities and fluctuation close to the experimental results of Kitsikoudis et al. (2017). Most of the numerical domain is within 10% deviation of the experimental results for the time-averaged velocity. The velocity fluctuations is overall underestimated in the flow field, but the largest part is also within 10% of the normalized velocity fluctuations. For both the time-average velocities and fluctuations is the same pattern visible in the flow field. The time-average velocities differ most close to the bottom and cylinder, where the velocities are harder to measure. Further, is a RANS-simulation not able to resolve all turbulence, which is one of the main reasons that the turbulence is underestimated.

5.2 Effect of inclination close to the cylinder and the bed

In this section, simulation 1 and 2 have been compared to each other. The flat bed simulations with different inclination angles are compared in order to answer the second research question. The second research question is:

"How does the inclination of a cylinder affect the flow structure close to the cylinder and bed?"

The inclination of a cylinder does affect the flow structure near the cylinder and the bed. The alterations change the flowfield upstream of the cylinder and influence how the flow crosses the cylinder. Further, alters the inclination the wake and different velocity components dominate the flow structure. Upstream of the cylinder the flow is bended downwards for an straight cylinder. For an inclined cylinder the flow also bends upwards, which weakens the HV. After the flow is bended,

the flow crosses the cylinder perpendicular, even close to the bottom. In the wake downstream of the cylinder a clear upflow is noticed. The inclination affects the well-defined lee-wake vortices, for a straight cylinder these are distinctive. The lee-wake vortices do not play a role in the inclined cylinder case. The wake of the inclined cylinder is much more unstructured and 3D mixing plays a larger role, compared to the wake of the straight cylinder. This also makes that in the inclined case no clear upflow behind the cylinder is present. Close to the bottom the reconnection of the HV is visible, as it result in large time-averaged velocity fluctuations. Far from the bed and cylinder the inclination affects that the turbulence shifts from streamwise and transverse direction towards more in vertical direction. Overall the inclination decreases the fluctuations in the velocity, which also lead to a decrease in Turbulent Kinetic Energy (TKE).

5.3 Effect of scour and inclination angle on the flow field

In this section, simulation 3 and 4 have been compared to each other. These scour simulation have different inclinations angles, which can be used how the scour affects the flow structure around a straight and inclined cylinder. The results are used to answer the third research question, which is:

"How does scour affect the flow structure around a straight and inclined circular cylinder?"

The inclination around a scoured bottom does change the flow field. Upstream of the cylinder the flow field bends more downward into the scour hole. As for the inclined cylinder with a flat bed, also with a scoured bed the flow is bended upward in front of the cylinder. So the HV is weakened again compared to the straight cylinder cases.In both simulation is the HV inside the scour hole. Due to the scour hole the flow crosses the cylinder not perpendicular, but slightly angled. Where for an inclined cylinder it is again perpendicular. Compared to the flat bed cases there is no reconnection of the HV. Downstream of the cylinder the wake is much more unstructured for a straight cylinder compared to a flat bed. Further decreases the TKE for an inclined cylinder compared to a straight cylinder. The velocity fluctuations downstream happen mainly close to the cylinder, where for the flat bed cases the fluctuations were further away from the cylinder. The main contributor for the TKE is now the transverse direction, which was also the case for simulation 1 with a straight cylinder. Overall the TKE of simulation 3 has decreased compared to simulation 1. Simulation 4 has some discrepancies. There are very high velocities at the bottom and large pressure gradients present in the simulation. But in general a decrease of the TKE is clearly visible.

5.4 Effects on the bed shear stress

The other research questions focused on the effect on the flow field, but the last sub research question focuses on the bed shear stress. To answer the research questions all 4 simulations have been compared. The last sub question is:

"How does scour and inclination affect the bed shear stress?"

The scour and inclination do affect the bed shear stress amplification upstream of the cylinder and at the sides. Downstream of the cylinder the bed shear stress fluctuations are dominant, but the effect of scour and bending is much smaller on the fluctuations. From the second and third sub

research question we can understand due to the inclination part of the flow field is bended upward, reducing the strength of the HV. This is also visible in the comparison between simulations at a rigid bed with a straight and inclined cylinder. The weaker HV reduces the shear stresses on the bed. This results lower bed shear stresses at the inclined case. Furthermore, the bed shear stress is more elongated, as the streamlines contract near the cylinder, as well as the contraction behind the cylinder, caused by the flow that crosses the cylinder perpendicular. As the scour holes are in equilibrium condition, the bed shear stress has decreased. This is also the case between simulation 1 and 3 (straight cylinder, with/without scour) and between 2 and 4 (inclined, with/without scour). The HV now has the largest impact on the bed shear stress, because there can be seen that the maximum bed shear stress now shifts more upstream in front of the cylinder. For simulation 1 the contraction of the streamlines played an important role and the largest bed shear stresses were at the sides of the cylinder. Further are the velocities higher at the hills of the sediment deposition area downstream of the scour hole for both simulation 3 and 4, where locally the bed shear stresses are higher. This is even more the case for simulation 4, where the velocities at the bottom are even higher. In general no clear indication is present that the inclination of the cylinder does decrease the bed shear stress between simulation 3 and 4 as there is an increase in amplification. The bed shear stress fluctuations are for all scenarios mainly downstream of the cylinder. The fluctuations vary mainly between $0.5\tau^*_{rms}$ and $1.3\tau^*_{rms}$. Between the straight cylinder and inclined cylinder at a flat bed, a small reduction of $0.2\tau^*_{rms}$ is visible. This is much smaller than the reduction in the normalized time-averaged bed shear stress.

5.5 The effect of vegetation

In the previous sections the sub-research questions have been answered. These conclusions are needed in order to answer the main research question, which is:

"How does the bending of vegetation and scour of the bottom affect the flow structure and bed shear stress?"

Based on the previous sub-research questions, there can be concluded that the bending of vegetation affects the flow structure and the bed shear stress. The bending of vegetation results in flow crossing the vegetation perpendicular, resulting in downward flow at the stem and upward flow behind the vegetation. Furthermore decreases the turbulent kinetic energy caused by the vegetation with inclination in downstream direction. These differences in the flow structure affects the bed shear stress, which decreases for an inclined cylinder compared to an upright cylinder. Also the orientation of the maximum amplification shift, as the flow crosses the cylinder perpendicular, at a larger polar angle of the cylinder the flow contracts. The contraction results in a more elongated area with a higher bed shear stress compared to the straight cylinder. These bed shear stresses will erode the bed, as has been measured by Kitsikoudis et al. (2017). The equilibrium conditions of the bed also impact the flow structure. Where for the flat bed and straight cylinder the vortex shedding was periodic, after either inclination or a scoured bed the processes become more a-periodic and unstructured. No clear lee-wake vortices can be detected. However, for the scoured bed and a straight cylinder the flow becomes more streamlined and has behaviour of an inclined cylinder. The wake length increases over depth, as also is the case for the inclined case. Furthermore the pressure difference decreases for both cases, which also indicates a more streamlined case. Beside a locally

large TKE the inclination of a vegetation and a scour hole also decreases the TKE, especially further downstream of the vegetation.

5.6 Recommendations

Based on the different simulations, between the flat bed straight and inclined cylinder a large decrease in bed shear stress is visible. There are different limitations in this study. One important factor is that waves are not included. These waves would result in swaying of the vegetation, resulting in a loss of energy in the water. However that will be difficult to model, so I suggest to focus on the bending angle of vegetation. Therefore, it is recommended to include the flexibility of vegetation in the simulation and experiments. The flexibility is beneficial for reducing the bed shear stress and should thus be taken into consideration. The conditions in for example a salt marsh are different than steady turbulent flow, but the general concept of that inclination influences the bed shear stress is still very good applicable and has a large effect. In reality the stem will be likely bend with the flow, where if the velocity of the flow increases the bending increases. Therefore a more realistic representation of vegetation. A 3D-model of a single plant can be implemented in the snappyHexMesh model. This would therefore not only include the effects of the stem, but the leaves as well. This also leads to the second recommendation to understand the relation between the bending of the vegetation and the flow velocity, which has to be studied with experiments. In this case a relatively high velocity and diameter size have been used, where even the Reynolds number is relatively high for flow in vegetation. To get a more realistic understanding of effect of the bent vegetation, it is important to understand how the bending is related to the flow velocity.

Another recommendation based on the modelling of vegetation is to understand the effect of multiple inclined vegetation. The Equations that are nowadays used are often validated based on experiments with straight cylinders, for example in Baptist et al. (2007). In this study can be seen that the flow is more streamlined around inclined cylinder, meaning that the TKE decreases and that the flow is less affected by the cylinder. Therefore the bending of vegetation is important to take into account for flexible vegetation. To understand the effect on multiple inclined cylinders there are two options, one being experimental and the other being numerical. In case of a numerical simulation, the recommendation would be to do it based on the methodology of multiple cylinders as in Etminan et al. (2018). In case of experimental simulations depends a lot on if the stems are fully submerged or not as well as on which parameter will be researched. For example to investigate the effect on vegetation resistance, the methodology of Baptist et al. (2007) would be useful. This will give insights in the effect of bent vegetation in a salt marsh and give more qualitative depth in how to manage salt marshes where vegetation is flexible.

In a broader sense, so for hydraulic engineering the implementation of the cylinder in water can still be further explored. Especially since the RANS-simulation are not able to capture all turbulent structures, there is still a large opportunity to research this. To capture more of the turbulent structures a DES-simulation of inclined cylinder would be recommended. These simulations capture the turbulence better than RANS. Given the trouble that snappyHexMesh gave due to the way of refining and that the implementation of a scour hole is not feasible with only blockMesh. There are two options to solve this. The best option is to use another meshing program for the grid that is

able to generate smooth transitions as well as the layers that can be added along the cylinder and bottom. The second option would be to use blockMesh, but with a simplified version of a scour hole. The first option is preferred as this will yield more accurate results on the simulation and is a more realistic scenario. Furher, the implementation of a DES-model could give more quantitive knowledege on how the flow behaves around inclined cylinder. The largest vortices are modelled using RANS, but the smaller vortices that appear inside the scour hole can further be investigated.

Acknowledgement

This work was carried out on the Dutch national e-infrastructure with the support of SURF Cooperative.

Chapter 6

List of symbols

Symbol	Description	Unit
Co	Courant number	–
Re	Reynolds number	–
D	Diameter of the cylinder	m or cm
I	Turbulence Intensity	–
l	turbulent length scale	m
p	Pressure	Pa
p_k	Kinematic pressure	m^2/s^2
u	Streamwise velocity	m/s
$\overline{u}$	Time-averaged streamwise velocity	m/s
u'	Velocity fluctuation	m/s
u_0	Depth average velocity	m/s
u_τ	Friction velocity	m/s
v	Transverse velocity	m/s
w	Vertical velocity	m/s
y^+	Dimensionless wall distance	–
δ_{ij}	Kronecker delta	–
ϵ	Turbulent kinetic energy dissipation	m^2/s^3
k	Model turbulent kinetic energy	m^2/s^2
ν	Kinematic viscosity	m^2/s^2
ν_t	Turbulent viscosity/eddy viscosity	m^2/s
ρ	Density	kg/m^3
τ	Bed shear stress	m^2/s^2
ω	Turbulence specific dissipation rate	$1/s$
S_{ij}	Mean strain-rate tensor	$1/s$
TKE	Turbulent Kinetic Energy	m^2/s^2

Table 6.1: List of variables. A * denotes a dimensionless version of the variable.

Chapter 7

List of abbreviations

Abbreviation	**Full word**
BC	Boundary Conditions
CFD	Computational Fluid Dynamics
DEM	Digital Elevation Model
DES	Detached Eddy Simulation
DNS	Direct Numerical Simulation
HV	Horseshoe vortex
IC	Initial Conditions
LES	Large Eddy Simulation
RANS	Reynolds-Averaged Navier-Stokes
TKE	Turbulent Kinetic Energy

Table 7.1: List of Abbreviations

References

Aksel, M. (2023). Numerical Analysis of the Flow Structure around Inclined Solid Cylinder and Its Effect on Bed Shear Stress Distribution. *Journal of Applied Fluid Mechanics*, *16*(8), 1627–1639. https://doi.org/10.47176/jafm.16.08.1697

Aksel, M., Yagci, O., Kirca, V. S., Erdog, E., & Heidari, N. (2021). A comparative analysis of coherent structures around a pile over rigid-bed and scoured-bottom. *Ocean Engineering*, *226*. https://doi.org/10.1016/j.oceaneng.2021.108759

ANSYS Inc. (2009). *ANSYS FLUENT 12.0 User's Guide* (tech. rep.).

Baptist, M. J. (2003). *International workshop on RIParian FORest vegetated channels: hydraulic, morphological and ecological aspects A flume experiment on sediment transport with flexible, submerged vegetation* (tech. rep.).

Baptist, M. J., Babovic, V., Uthurburu, J. R., Keijzer, M., Uittenbogaard, R. E., Mynett, A., & Verwey, A. (2007). On inducing equations for vegetation resistance. *Journal of Hydraulic Research*, *45*(4), 435–450. https://doi.org/10.1080/00221686.2007.9521778

Baptist, M. J., van den Bosch, L. V., Dijkstra, J. T., & Kapinga, S. (2005). Modelling the effects of vegetation on flow and morphology in rivers. *Large Rivers*, *15*(1-4), 339–357. https://doi.org/10.1127/lr/15/2003/339

Baykal, C., Sumer, B. M., Fuhrman, D. R., Jacobsen, N. G., & Fredsoe, J. (2015). Numerical investigation of flow and scour around a vertical circular cylinder. *Philosophical Transactions of the Royal Society A: Mathematical, Physical and Engineering Sciences*, *373*(2033). https://doi.org/10.1098/rsta.2014.0104

Chang, W. Y., & Constantinescu, G. (2023). Oscillatory flow around a vertical circular cylinder placed in an open channel: Coherent structures, sediment entrainment potential and drag forces. *Journal of Fluid Mechanics*, *964*. https://doi.org/10.1017/jfm.2023.367

Conde-Frias, M., Ghisalberti, M., Lowe, R. J., Abdolahpour, M., & Etminan, V. (2023). The Near-Bed Flow Structure and Bed Shear Stresses Within Emergent Vegetation. *Water Resources Research*, *59*(4). https://doi.org/10.1029/2022WR032499

Du, S., Liang, B., & Lee, D. Y. (2019). Numerical investigation of local scour with inclined piles. *Journal of Coastal Research*, *91*(sp1), 161–165. https://doi.org/10.2112/SI91-033.1

Etminan, V., Ghisalberti, M., & Lowe, R. J. (2018). Predicting Bed Shear Stresses in Vegetated Channels. *Water Resources Research*, *54*(11), 9187–9206. https://doi.org/10.1029/2018WR022811

Etminan, V., Lowe, R. J., & Ghisalberti, M. (2017). A new model for predicting the drag exerted by vegetation canopies. *Water Resources Research*, *53*(4), 3179–3196. https://doi.org/10.1002/2016WR020090

Graf, W. H., & Istiarto, I. (2002). Flow pattern in the scour hole around a cylinder. *Journal of Hydraulic Research*, *40*(1), 13–20. https://doi.org/10.1080/00221680209499869

Greenshields, C., & Weller, H. (2022, April). Notes on Computational Fluid Dynamics: General Principles. https://doc.cfd.direct/notes/cfd-general-principles/

Guerrero. (2021). Turbulence modeling in OpenFOAM: Theory and applications. https://www.wolfdynamics.com/training/turbulence/OF2021/turbulence_2021_OF8.pdf

Kazhdan, M., & Hoppe, H. (2013). Screened poisson surface reconstruction. *ACM Transactions on Graphics*, *32*(3). https://doi.org/10.1145/2487228.2487237

King, A. T., Tinoco, R. O., & Cowen, E. A. (2012). A k-ϵ turbulence model based on the scales of vertical shear and stem wakes valid for emergent and submerged vegetated flows. *Journal of Fluid Mechanics*, *701*, 1–39. https://doi.org/10.1017/jfm.2012.113

Kirkil, G., Asce, S. M., Constantinescu, ; S. G., Asce, M., & Ettema, R. (2008). Coherent Structures in the Flow Field around a Circular Cylinder with Scour Hole. https://doi.org/10.1061/ASCE0733-94292008134:5572

Kitsikoudis, V., Kirca, V. S., Yagci, O., & Celik, M. F. (2017). Clear-water scour and flow field alteration around an inclined pile. *Coastal Engineering*, *129*, 59–73. https://doi.org/10.1016/j.coastaleng.2017.09.001

Liu, M., Zhang, S., Li, Y., & Qin, J. (2024). Numerical investigation of flow over a finite length inclination circular cylinder under Re = 3900. *Ocean Engineering*, *300*. https://doi.org/10.1016/j.oceaneng.2024.117262

Liu, Y., Huang, M., & Jian. (2024). Numerical simulation of local scour around an inclined monopile in steady current. *IOP Conference Series: Earth and Environmental Science*, *1334*(1). https://doi.org/10.1088/1755-1315/1334/1/012007

Menter, F. R. (1993). *AIAA 93 · 2906 Zonal Two Equation k · co Turbulence Models for Aerodynamic Flows. ZONAL TWO EQUATION k-w TURBULENCE MODELS FOR AERODYNAMIC FLOWS* (tech. rep.).

Nepf, H., & Ghisalberti, M. (2008). Flow and transport in channels with submerged vegetation. https://doi.org/10.2478/s11600-008-0017-y

OpenFOAM The Open Source CFD Toolbox User Guide (tech. rep.). (2024).

OpenCFD Team & Nagy, J. (2025). OpenFOAM: User Guide online. https://www.openfoam.com/documentation/guides/latest/doc

Roulund, A., Sumer, B. M., Fredsøe, J., & Michelsen, J. (2005). Numerical and experimental investigation of flow and scour around a circular pile. *Journal of Fluid Mechanics*, *534*, 351–401. https://doi.org/10.1017/S0022112005004507

Spalart, P. R. (2009). Detached-eddy simulation. https://doi.org/10.1146/annurev.fluid.010908.165130

Tang, C., Lei, J., & Nepf, H. M. (2019). Impact of Vegetation-Generated Turbulence on the Critical, Near-Bed, Wave-Velocity for Sediment Resuspension. *Water Resources Research*, *55*(7), 5904–5917. https://doi.org/10.1029/2018WR024335

Tang, J., Chen, Y., Shen, Y., & Cao, S. (2024). Numerical study on stem-generated turbulence due to emergent rigid vegetation in water waves. *Ocean Engineering*, *304*. https://doi.org/10.1016/j.oceaneng.2024.117940

Temmerman, S., Horstman, E. M., Krauss, K. W., Mullarney, J. C., Pelckmans, I., & Schoutens, K. (2023). Marshes and Mangroves as Nature-Based Coastal Storm Buffers. https://doi.org/10.1146/annurev-marine-040422

van Veelen, T. J., Nepf, H., Hulscher, S. J., & Borsje, B. W. (2025). The thresholds of sediment resuspension within emergent vegetation under combined wave-current conditions – a flume experiment. *Coastal Engineering*, 104727. https://doi.org/10.1016/j.coastaleng.2025.104727

Vargas-Luna, A., Crosato, A., Calvani, G., & Uijttewaal, W. S. (2016). Representing plants as rigid cylinders in experiments and models. *Advances in Water Resources*, *93*, 205–222. https://doi.org/10.1016/j.advwatres.2015.10.004

Wang, S., Yang, S., He, Z., Li, L., & Xia, Y. (2020). Effect of inclination angles on the local scour around a submerged cylinder. *Water (Switzerland)*, *12*(10), 1–20. https://doi.org/10.3390/w12102687

Wilcox, D. C. (2010). *Turbulence modeling for CFD*. DCW Industries.

Zanke, U. C. E. (2003). On the influence of turbulence on the initiation of sediment motion. *International Journal of Sediment Research*, *18*. https://www.researchgate.net/publication/228606993

Zhao, M., Cheng, L., & Zhou, T. (2009). Direct numerical simulation of three-dimensional flow past a yawed circular cylinder of infinite length. *Journal of Fluids and Structures*, *25*(5), 831–847. https://doi.org/10.1016/j.jfluidstructs.2009.02.004

Appendix A

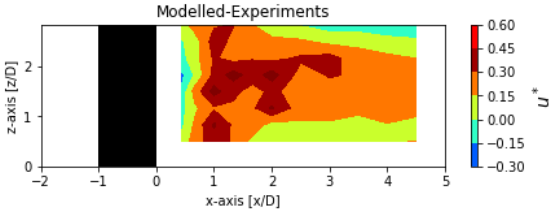

Figure A.1: Normalized time-averaged velocity difference between the experiments and simulations

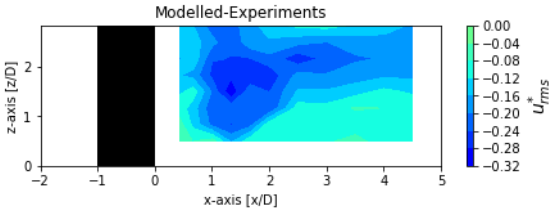

Figure A.2: Normalized time-averaged velocity fluctuation difference between the experiments and simulations

Appendix B

Mesh quality control	Value
maxNonOrtho	75
maxBoundarySkewness	20
maxInternalSkewness	4
maxConcave	80
minVol	1.00E-13
minTetQuality for the mesh	1e-15
minTetQuality for the added layers	1e-30
minArea	-1
minTwist	0.02
minDeterminant	0.001
minFaceWeight	0.05
minVolRatio	0.01
minTriangleTwist	-1
minFlatness	0.5
nSmoothScale	4
errorReduction	0.75

Table B.1: Values for the mesh requirements in snappyHexMesh

Appendix C

C.1 Simulation 1: Straight cylinder with flat bed

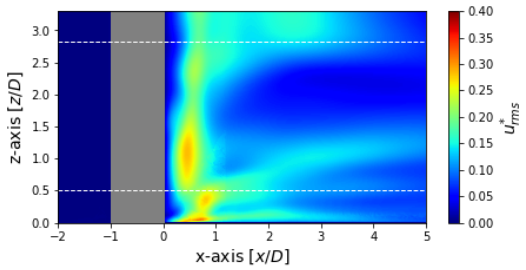

(a) Normalized streamwise velocity fluctuations

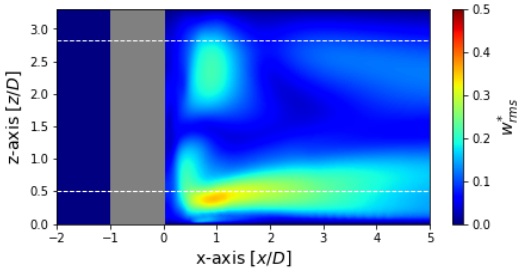

(b) Vertical velocity fluctuations

C.2 Simulation 2: Inclined cylinder with flat bed

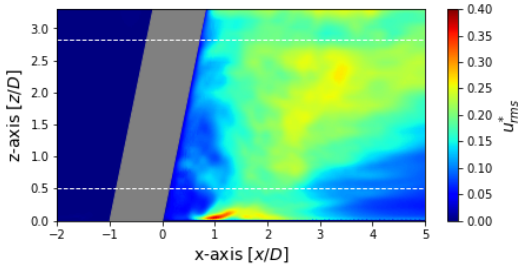

(a) Normalized streamwise velocity fluctuations

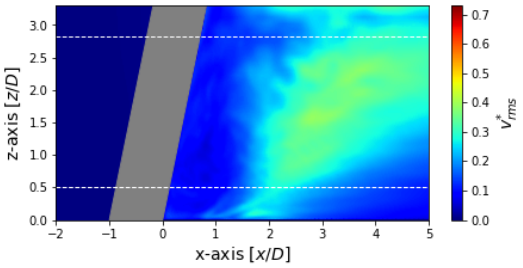

(b) Normalized transverse velocity fluctuations

C.3 Simulation 3: Straight cylinder with scoured bed

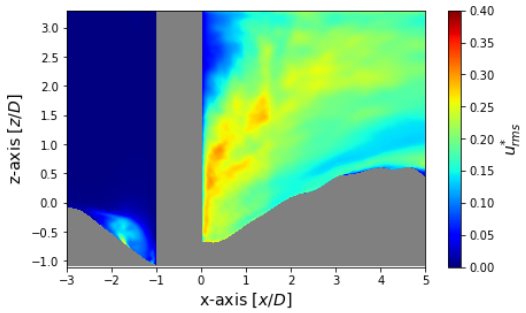

(a) Normalized streamwise velocity fluctuations

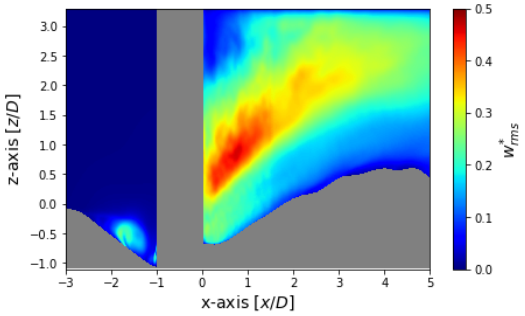

(b) Normalized vertical velocity fluctuations

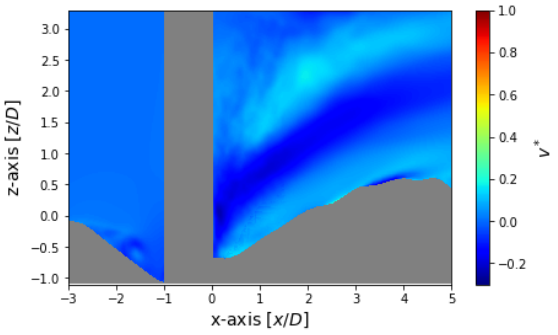

Figure C.4: Normalized vertical velocity

C.4 Simulation 4: Inclined cylinder with scoured bed

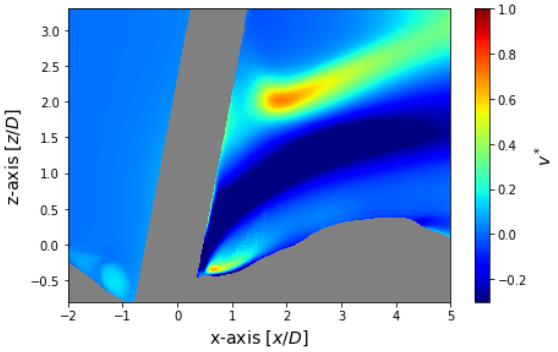

Figure C.5: Normalized transverse velocity